Quantum Hall conductance and de Haas–van Alphen oscillation in a tight-binding model with electron and hole pockets for $(TMTSF)_2NO_3$

Keita Kishigi
Faculty of Education, Kumamoto University, Kurokami 2-40-1, Kumamoto, 860-8555, Japan

Yasumasa Hasegawa
Department of Material Science, Graduate School of Material Science, University of Hyogo, Hyogo, 678-1297, Japan
(Received 14 March 2016; revised manuscript received 18 July 2016; published 4 August 2016)

Quantized Hall conductance and de Haas–van Alphen (dHvA) oscillation are studied theoretically in the tight-binding model for $(TMTSF)_2NO_3$, in which there are small pockets of electrons and holes due to the periodic potentials of anion ordering in the a direction. The magnetic field is treated by hoppings as complex numbers due to the phase caused by the vector potential, i.e., Peierls substitution. In realistic values of parameters and the magnetic field, the energy as a function of the magnetic field (Hofstadter butterfly diagram) is obtained. It is shown that the energy levels are broadened and the gaps are closed or almost closed periodically as a function of the inverse magnetic field, which is not seen in the semiclassical theory of the magnetic breakdown. The Hall conductance is quantized with an integer obtained by the Diophantine equation when the chemical potential lies in an energy gap. When electrons or holes are doped in this system, the Hall conductance is quantized in some regions of a magnetic field but it is not quantized in other regions of a magnetic field due to the broadening of the Landau levels. The amplitude of the dHvA oscillation at zero temperature decreases as the magnetic field increases, while it is constant in the semiclassical Lifshitz Kosevich formula.

DOI: 10.1103/PhysRevB.94.085405

I. INTRODUCTION

Organic conductors $(TMTSF)_2X$, where TMTSF is tetramethyl-tetra-selena-fulvalence and X is an anion ($X = NO_3$, PF_6, ClO_4, etc.) [1,2], have the structure of stacked planer molecules, TMTSF, in the a direction as shown in Fig. 1(a). We can neglect the hoppings perpendicular to a-b plane, because they are very small [1]. The energy band structure is well described [1] by six hopping integrals (t_{S1}, t_{S2}, t_{I1}, t_{I2}, t_{I3}, and t_{I4}), which are shown in Fig. 1(a). Since the absolute values of the hoppings in the chain along the a direction are about ten times larger than those between chains, the Fermi surface consists of quasi-one-dimensional sheets as shown in Fig. 2(a).

The unit cell of $(TMTSF)_2NO_3$ is doubled along the a direction due to the ordering of the orientation of the anion NO_3 below $T_{AO} \simeq 45$ K [3–5]. The Brillouin zone is halved and there appear small electron and hole pockets, as seen in Fig. 2(b). When the magnetic field (H) is applied perpendicular to the a-b plane, the energy of electrons is quantized. In this case, the de Haas–van Alphen (dHvA) effect [6] is expected. Fortin and Audourad [7,8] adopt the phenomenological network model [9,10] of a semiclassical theory for the magnetic breakdown and a semiclassical quantization of energies [11]. In two-dimensional systems, the oscillation of the chemical potential as a function of a magnetic field cannot be neglected in general [6,12–15], whereas it is safely neglected in the dHvA effect in three-dimensional systems as in the Lifshitz-Kosevich (LK) formula [6,13–20]. Fortin and Audourad [7,8] have shown that the oscillation of the chemical potential is very small and the LK formula explains the field and temperature dependencies of the amplitudes of the dHvA oscillation, if the effective masses of electrons and holes are nearly the same.

In a tight-binding model, the energy under a magnetic field can be obtained without a phenomenological parameter for the probability amplitude of the tunneling, which is used in the semiclassical theory of the magnetic breakdown. The quantized Landau levels of the two-dimensional free electrons are described by delta functions. When periodic potentials exist or the tight-binding model is used [21,22], the energy levels are broadened. These energy levels as a function of the magnetic field are known as the Hofstadter butterfly diagram [23–25]. The study of the dHvA oscillation has been done in the tight-binding model [26–30] in systems where a quasi-one-dimensional Fermi surface and a two-dimensional Fermi surface coexist. This Fermi surface is suitable to study the magnetic breakdown in the dHvA oscillation and is realized, for example, in κ-$(BEDT\text{-}TTF)_2Cu(NCS)_2$ [1]. Fortin and Ziman [31] have calculated the dHvA oscillation in a similar system by using the network model [9,10]. In both studies, the tight-binding model and the semiclassical network model, a combination frequency, $\beta - \alpha$, has been obtained due to the chemical potential oscillation as a function of the magnetic field.

The dHvA oscillation in the tight-binding model [32,33] for $(TMTSF)_2NO_3$ has been studied theoretically. The model studied previously was, however, a more simplified one and exaggerated parameter values were used (half-filled band on the rectangular lattice with $t_b/t_a = 0.6$ and $t'_b/t_a = 0.2$, where t_a and t_b are the nearest-neighbor hoppings in a and b directions, respectively, and t'_b is the next-nearest-neighbor hopping in b direction). On the other hand, the quantum Hall effect in $(TMTSF)_2NO_3$ has never been studied in the actual parameters in the tight-binding model, as far as we know. The integer quantum Hall effects in two-dimensional electron systems are understood as topological phenomena. The quantized value of the Hall conductance is obtained as a first Chern number or the solution of the Diophantine equation [34–36].

In this paper, we adopt the tight-binding model with the realistic parameters for $(TMTSF)_2NO_3$ in the magnetic field treated quantum mechanically. In experimentally accessible magnetic fields ($\sim$6 T), we obtain an interesting structure of the

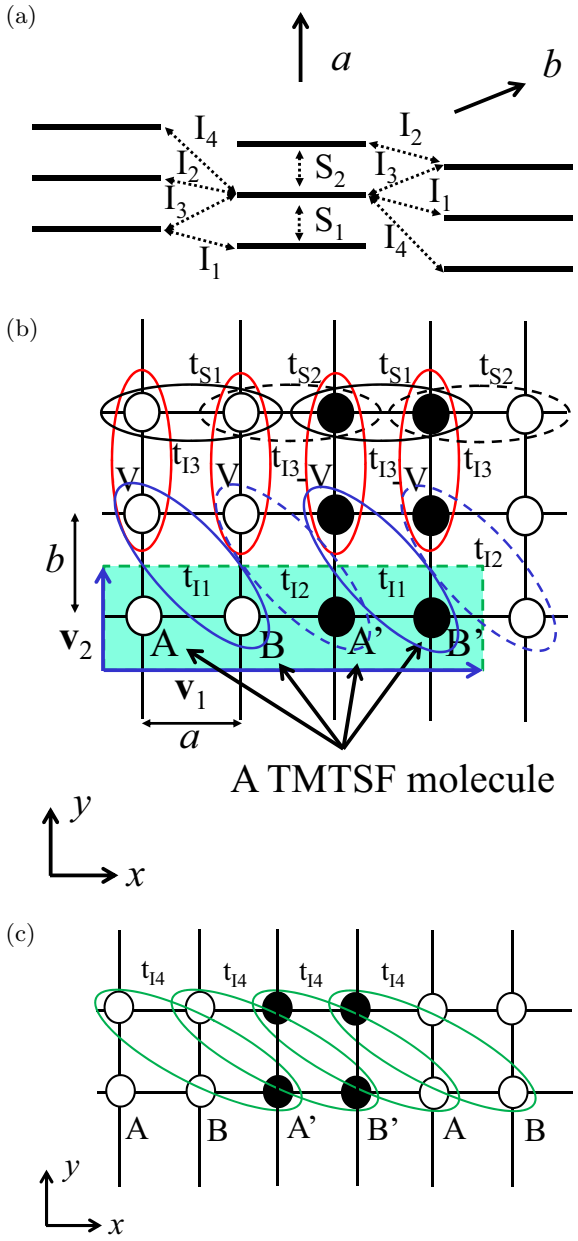

FIG. 1. (a) Schematic side view of $(TMTSF)_2X$. Solid lines are for TMTSF molecules and dotted lines are transfer integrals [1]. (b) The simplified tight-binding model for $(TMTSF)_2X$ in the rectangular lattice, where $2a$ and b are the lattice constants (note that there are two sites (A and B) in the unit cell when $V = 0$; the definition of a is a half of that used in Ref. [1]). The unit cell is shown as the light green rectangle. The transfer integrals (t_{S1}, t_{S2}, t_{I1}, t_{I2}, t_{I3}) are shown as ovals. The effect of the ordering of the orientation of the anion NO_3 is modeled by the on-site potentials $\pm V$. (c) Transfer integrals of t_{I4}.

energy as a function of the magnetic field (Hofstadter butterfly diagram), quantum Hall conductance, and dHvA oscillations. We show the difference between the results in the quantum-mechanical theory and those in the semiclassical theory.

II. SPIN-DENSITY WAVE IN $(TMTSF)_2NO_3$

The shape and the dimensionality of the Fermi surface in $(TMTSF)_2NO_3$ are controversial at high pressure and strong

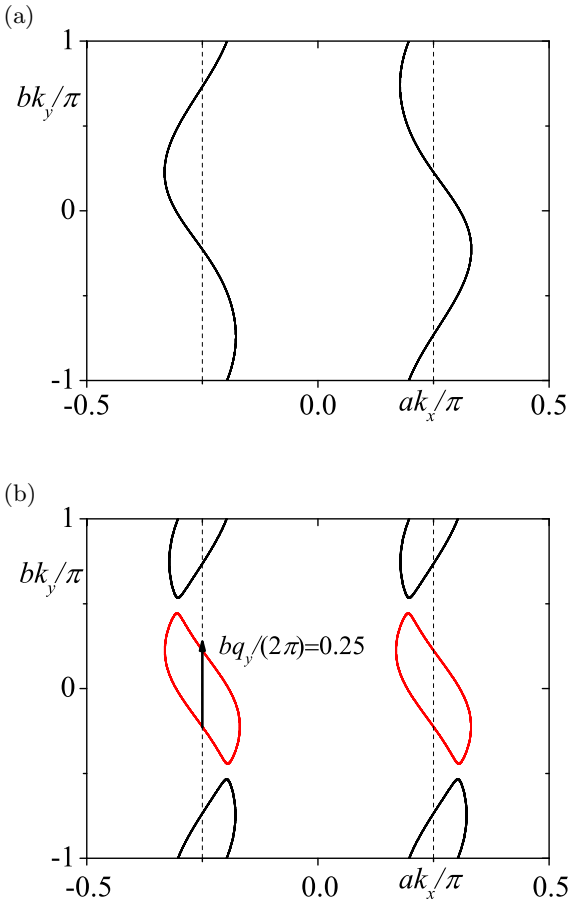

FIG. 2. (a) Fermi surface at 3/4-filling for $V = 0$ and the transfer integrals are $t_{S1} = 274.4$, $t_{S2} = 250.5$, $t_{I1} = -29.1$, $t_{I2} = -42.7$, $t_{I3} = 56.6$, and $t_{I4} = -6.3$ meV. (b) Fermi surface at 3/4-filling for $V = 12.38$ meV. The Brillouin zone is halved ($-1/4 < ak_x/\pi \leqslant 1/4$). Black and red curves are electron and hole pockets, respectively.

magnetic fields [4,5]. At the ambient pressure, the spin-density wave (SDW) [37–40] is stabilized in $(TMTSF)_2NO_3$ below $T_{SDW} \simeq 9 \sim 12$ K. The wave vector of the SDW has been observed in NMR experiments [41,42] to be $(q_x,q_y) \simeq (0,0.25(2\pi/b))$. That vector is indicated by an arrow in Fig. 2(b), which is a good nesting vector. By applying pressure, the nesting of the Fermi surface becomes less perfect and SDW is suppressed. Indeed, a metallic state in the absence of SDW is reported above 8.5 kbar in the magnetoresistance experiment by Vignolles *et al.* [4]. The orientational order of NO_3 occurs even at high pressure. They have shown the difference between the frequency of the Shubnikov–de Haas (SdH) oscillations at low pressures and at high pressures (above 8.5 kbar). They suggested that there exist two-dimensional pockets even above 8.5 kbar. However, Kang and Chung [5] have observed that the angular-dependent magnetoresistance oscillations in $(TMTSF)_2NO_3$ at 14 T and pressures of 6.0, 7.0, and 7.8 kbar are similar to those in $(TMTSF)_2ClO_4$. They suggested that $(TMTSF)_2NO_3$ in the metallic state at high pressure has a quasi-one-dimensional Fermi surface even in the presence of the anion ordering.

The theoretical study of the angular-dependent magnetoresistance, however, has been done only semiclassically

in quasi-one-dimensional systems [43–47] and quasi-two-dimensional systems [48]. The SdH oscillation has not been studied quantum mechanically in $(TMTSF)_2NO_3$, either. As we will show below, we study the tight-binding model for $(TMTSF)_2NO_3$ under a magnetic field at $T < T_{AO}$ without SDW order quantum mechanically and we obtain results that are not expected in the semiclassical theory. Therefore, in order to identify the shape and the dimensionality of the Fermi surface in $(TMTSF)_2NO_3$ at high pressures and the in presence of a magnetic field, we have to compare the experiments with a theory treated not at the semiclassical level but in quantum mechanics. Thus our study will be the first step to understand the shape and the dimensionality of the Fermi surface in $(TMTSF)_2NO_3$, where there are electron and hole pockets in the absence of magnetic field. Studies in the presence of the SDW order or under high pressure will be done in the future.

The field-induced spin-density wave (FISDW) has been also observed in $(TMTSF)_2NO_3$ at strong magnetic fields ($\sim$20 T) and at high pressure ($\sim$8.5 kbar) [4,5]. The FISDW is caused by electron-electron interactions in similar quasi-one-dimensional organic conductors such as $(TMTSF)_2PF_6$ and $(TMTSF)_2ClO_4$ [49,50]. Since the instabilities of the FISDW are expected to be strong in $(TMTSF)_2NO_3$, a study including electron-electron interactions needs to be done in the future.

III. ELECTRON AND HOLE POCKETS AT $H = 0$

Since the direction of the anion is random above T_{AO}, we can neglect the effects of the anion potential. Then, the tight-binding model for $(TMTSF)_2X$ is described by six hopping integrals, t_{S1}, t_{S2}, t_{I1}, t_{I2}, t_{I3}, and t_{I4}, which are shown in Fig. 1 [1]. Although the real lattice is monoclinic, the energy as a function of the wave number is topologically the same as that in the rectangular lattice as shown in Figs. 1(b) and 1(c). The energy as a function of the uniform magnetic field (Hofstadter butterfly diagram) is also the same. (A similar situation has been known to occur in the triangular lattice and the honeycomb lattice. For example, the tight-binding electrons on the triangular lattice have the same energy versus magnetic field as those on the square lattice with diagonal hoppings along one direction [24,25].) Since $t_{S1} \neq t_{S2}$ and $t_{I1} \neq t_{I2}$, there are two nonequivalent sites A and B in the unit cell. There are two bands in this case. Electrons are 3/4 filled for the bands made of the highest occupied molecular orbits (HOMO) of TMTSF, since one electron is removed from two TMTSF molecules. Then the lower band is completely filled and the upper band is half-filled. By diagonalizing Eq. (A20) (2×2 matrix) in Appendix A, we plot the Fermi surface in Fig. 2(a), in which we take the parameters reported by Alemany, Pouget, and Canadell [51]; $t_{S1} = 274.4$, $t_{S2} = 250.5$, $t_{I1} = -29.1$, $t_{I2} = -42.7$, $t_{I3} = 56.6$, $t_{I4} = -6.3$ meV.

The effect of the ordering of the anion NO_3 is taken into account as an on-site potential, V and $-V$, as shown in Fig. 1(b). In this case, there are four sites (A, B, A', and B') in the unit cell, which is indicated by a light green rectangle in Fig. 1(b); the unit cell becomes twice larger than without the anion ordering. The Brillouin zone is halved along k_x direction. The energy is obtained by the diagonalization of Eq. (A11) (4×4 matrix) in Appendix A. The minimum gap made at $(ak_x/\pi, bk_y/\pi) = (1/4, 1)$ between a third band and a fourth band is obtained to be about 17.80 meV when we set $V = 12.38$ meV. Alemany, Pouget, and Canadell [51] have obtained the minimum gap between the third band and the fourth band to be 17.8 meV. Therefore we take $\pm V = \pm 12.38$ meV as the on-site potential of $(TMTSF)_2NO_3$ at $T < T_{AO}$. We show the Fermi surface in Fig. 2(b) in the extended zone scheme, where there exist electron and hole pockets with the same area. When V becomes large, the areas of electron and hole pockets become small. In Figs. 3 and 4, we show the 3D plots and the contour plots of the third band and the fourth band as a function of the wave number $\mathbf{k}$ for $V = 12.38$ and 86.50 meV, respectively. When $V \geqslant 86.50$ meV, the areas of electron and hole pockets are zero.

IV. QUANTUM HALL EFFECT AND LANDAU QUANTIZATION

The energy of tight-binding electrons in a uniform magnetic field is obtained by taking the phase factor in the hoppings as shown in Appendix B. The energy can be calculated only when the magnetic flux (Φ) through the area of the unit cell ($4ab$) is a rational number p/q in the unit of the flux quantum (ϕ_0), where p and q are mutually prime numbers. Thus we define h as

$$h = \frac{\Phi}{\phi_0} = \frac{4abH}{\phi_0}, \tag{1}$$

and we take h as a rational number

$$h = \frac{p}{q}. \tag{2}$$

The value of the flux quantum is $\phi_0 = 2\pi\hbar c/e \simeq 4.14 \times 10^{-15}$ T m^2, where $2\pi\hbar$, c and e are the Planck constant, the speed of light and the absolute value of electron charge, respectively. Since $a \simeq 7.02$ Å and $b \simeq 7.54$ Å in $(TMTSF)_2NO_3$ [52], $h = 1$ corresponds to about $H = 1955$ T.

In the presence of a weak periodic potential [21,22], each Landau level is broadened (which is called Harper broadening) and separates into p bands when the magnetic flux Φ through the unit cell is $\Phi = (p/q)\phi_0$. On the other hand, the electron energy becomes q bands when the magnetic flux Φ is applied to the tight-binding electrons with one site and one orbit in the unit cell.

When the chemical potential is in the rth gap from the bottom in the tight-binding model, the quantized Hall conductance is given as

$$\sigma_{xy} = \frac{e^2}{h} t_r, \tag{3}$$

where the integer t_r is given by the Diophantine equation [34–36]:

$$r = q s_r + p t_r. \tag{4}$$

Two cases (the weak potential case and the tight-binding electrons) are reconciled, when $p/q \ll 1$ and the electron filling is small in the tight-binding model on a rectangular (or triangular, honeycomb, etc.) lattice; every set of p bands from the bottom of the energy is considered as a broadened Landau level, i.e., each Landau level is separated into p bands. The energy gaps above the (pt_r)th band from the bottom are larger than other energy gaps. When the chemical potential is in the

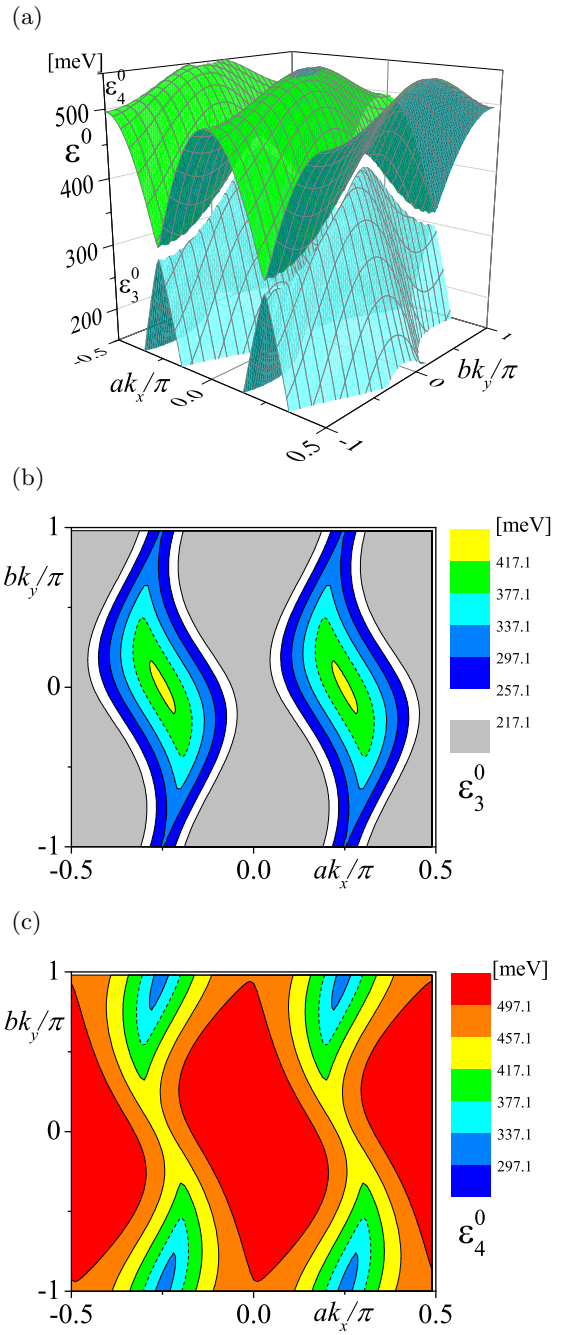

FIG. 3. (a) The third and fourth energy bands near the Fermi energy ($\varepsilon_F^0 \simeq 377.1$ meV) at 3/4-filling with the same parameters as those in Fig. 2(b) ($V = 12.38$ meV). In this case, the energy gap at $(ak_x/\pi, bk_y/\pi) = (1/4, 1)$ is $2\Delta \simeq 17.80$ meV, the top energy of the third band is $\varepsilon_{3t}^0 \simeq 425.3$ meV, and the bottom energy of the forth band is $\varepsilon_{4b}^0 \simeq 317.8$ meV. Contour plots of (b) the third energy band and (c) the fourth energy band. Dotted lines are for the Fermi surface at 3/4-filling.

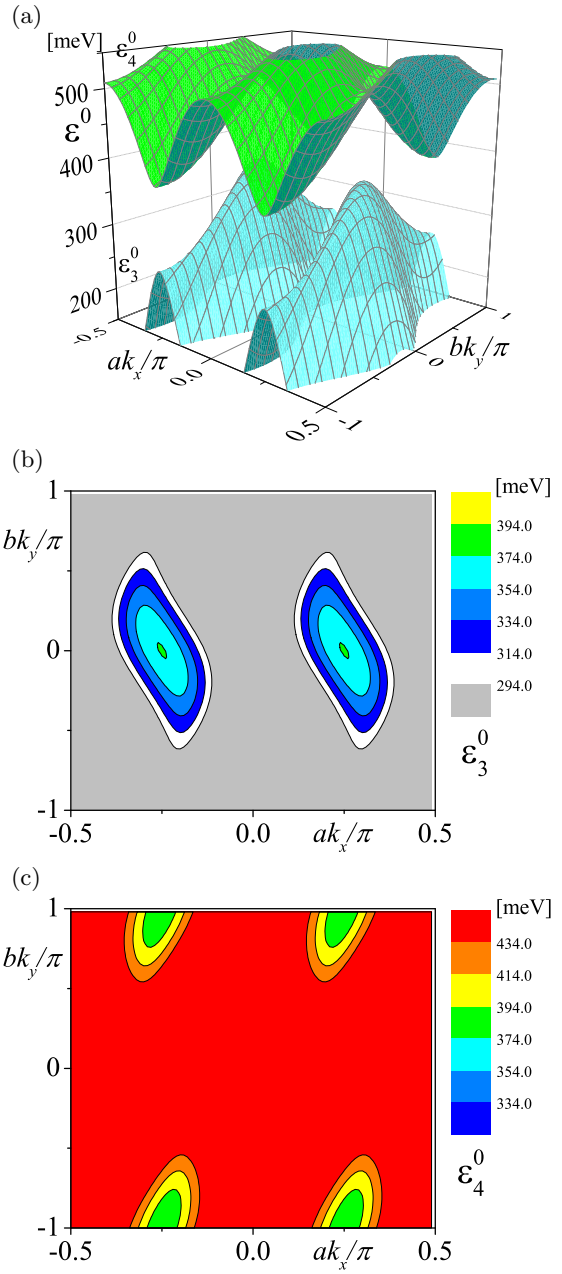

FIG. 4. (a) The third and fourth energy bands near the Fermi energy ($\varepsilon_F^0 \simeq 374.7$ meV) at 3/4-filling for $V = 86.50$ meV. Other parameters are the same as those in Fig. 2. Contour plots of (b) the third energy band and (c) the fourth energy band.

(pt_r)th gap from the bottom, $s_r = 0$. The Hall conductance given by t_r is understood as the result of the t_r Landau levels, each of which is broadened and separates into p sub-bands. The smaller $(p-1)$ gaps are considered as the gaps between the p bands within the t_rth Landau level, as in the weak potential case. In this way, the trivial value of the quantum Hall effect ($s_r = 0$) can be understood in the case Landau levels for free electrons,

$$\varepsilon_n^{\text{parabola}} \propto (n + \gamma^{\text{parabola}})h, \tag{5}$$

where n is zero or a positive integer and the phase is $\gamma^{\text{parabola}} = 1/2$. The Landau quantization of the energy levels [Eq. (5)] is obtained in the approximation that the energy dispersion near the bottom of the band at $h = 0$ is treated as that of free electrons, i.e., parabolic ($\varepsilon_{\mathbf{k}}^{(h=0)} \propto (k_x^2 + k_y^2)$). The Landau levels are obtained by the condition that the area of the Fermi surface at $h = 0$ is quantized [11] to be proportional to $(n +$

$\gamma)h$. We call this quantization as the semiclassical Landau quantization.

In order to observe nontrivial values of Hall conductance ($s_r \neq 0$) in the tight-binding electrons on rectangular and triangular lattices, a very strong magnetic field (the flux through the unit cell should be the same order as the flux quantum) is required. In the honeycomb lattice, which has two sites in the unit cell and there are $2q$ bands, the gaps labeled by $s_r = 1$ are also large at small magnetic field near half-filling [53]. The quantum Hall effect with $s_r = 1$ is observed in graphene when electrons or holes are doped [54]. The quantum Hall effect in graphene with $s_r = 1$ can be also understood semiclassically, if we approximate the energy dispersion near the massless Dirac points $[\pm\mathbf{k}^0 = \pm(k_x^0, k_y^0)]$ at $h = 0$ as

$$\varepsilon_{\mathbf{k}}^{(h=0)} \propto \pm\sqrt{\left(k_x - k_x^0\right)^2 + \left(k_y - k_y^0\right)^2} \tag{6}$$

and adopt the semiclassical quantization [11] of the area of the Fermi surface,

$$\varepsilon_n^{\mathrm{Dirac}} \propto \mathrm{sign}(n)\sqrt{(|n| + \gamma^{\mathrm{Dirac}})h}, \tag{7}$$

where n is integer and $\gamma^{\mathrm{Dirac}} = 0$. In the semiclassical treatment of Landau quantization, the broadening of the Landau levels and a rich structure of the Hofstadter butterfly diagram do not appear. In a real system of graphene, a very strong magnetic field is necessary to observe the quantum Hall effect for $s_r \neq 1$. However, when the area of the unit cell is large, the rich structure of the Hofstadter butterfly diagram can be observed experimentally at accessible magnetic fields. Indeed, the moire patterns in twisted bilayer graphene, graphene on hexagonal boron nitride (h-BN) substrates [55], graphene antidot lattices [56], cold atoms in optical lattices [57,58], etc., are shown to have a Hofstadter butterfly diagram with various values of s_r and t_r.

V. ENERGY IN THE MAGNETIC FIELD

By numerically diagonalizing the matrix of Eq. (B23), we plot the energy $\varepsilon_{i,\mathbf{k}}$ as a function of h in Fig. 5(a) for $(TMTSF)_2NO_3$ at $T > T_{AO}$, where the Fermi surface consists of two warped lines as shown in Fig. 2(a). There are $2q$ bands at $h = p/q$ and each band is doubly degenerate. Since the Fermi surface is not closed, the Landau quantization is not expected to occur near the Fermi energy in the semiclassical treatment [11]. Even in this case there should be some very small gaps in the tight-binding electrons in principle, but there are no visible gaps in the energy spectrum near 3/4-filling, as shown in Fig. 6. It is consistent with the semiclassical picture that the Landau quantization occurs only when the Fermi surface is closed. At $T < T_{AO}$, where the orientation of the anion orders, V is finite and electron and hole pockets appear at $h = 0$ as shown in Fig. 2(b). The Hofstadter butterfly diagrams for $V = 12.38$ meV and the three-times larger value ($V = 37.14$ meV) are shown in Figs. 5(b) and 5(c), respectively. The gaps are labeled by (s_r, t_r) [Eq. (4)] in Figs. 5(a)–5(c). The overall structures for $V \neq 0$, especially for smaller filling $[(s_r, t_r) = (0,1),(0,2),$ etc.], are similar to that for $V = 0$ [Fig. 5(a)]. We plot the Hofstadter butterfly diagram near the Fermi energy for the 3/4 filled case in Fig. 7 ($V = 12.38$ meV),

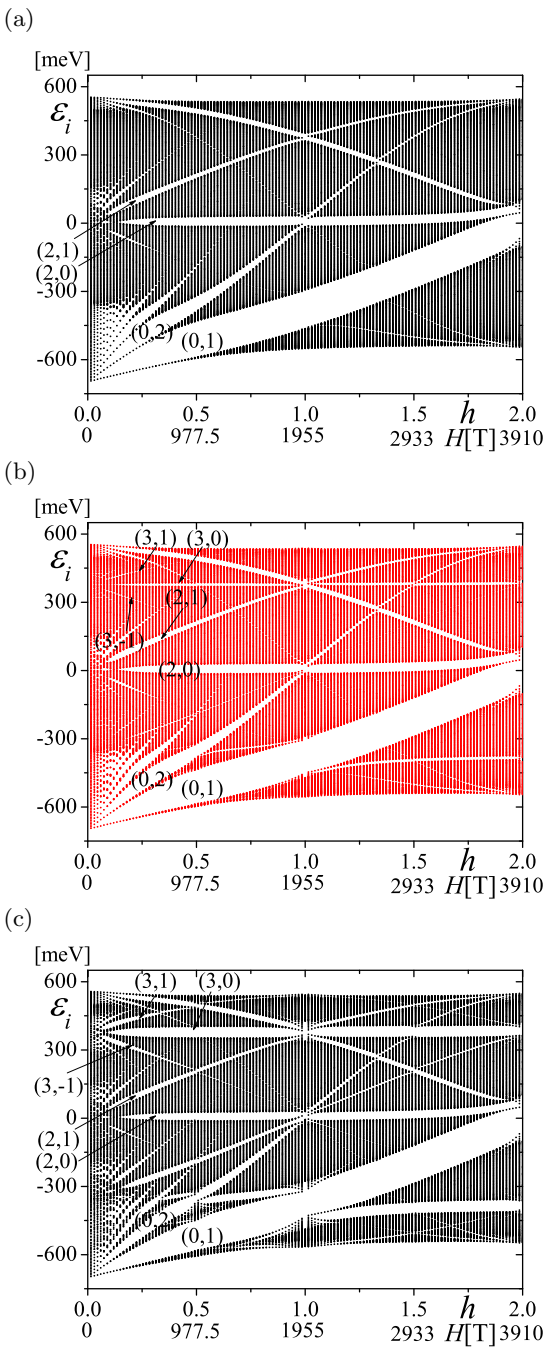

FIG. 5. Energy as a function of h. (a) Parameters are the same as those in Fig. 2(a) ($V = 0$). (b) Parameters are the same as those in Fig. 2(b) and Fig. 3 ($V = 12.38$ meV). (c) $V = 37.14$ meV and other parameters are the same as those in Fig. 2. We take $h = p/q$ with $q = 67$ and $p = 1,2,3,\ldots,2q$. Wave numbers are taken as $(k_x, k_y) = (0,0), (\pi/(2aq),0)$, and $(2\pi/(2aq),0)$. Other parameters are the same as those in Fig. 2. The quantum numbers (s_r, t_r) for some gaps are shown.

Fig. 10 ($V = 37.14$ meV), and Fig. 11 ($V = 86.50$ meV, no pockets).

In Fig. 7, the energy is not quantized as delta functions for a finite value of h, but we can see the broadened Landau levels starting from $\varepsilon_i = \varepsilon_{4b}^0$ and ε_{3t}^0 at $h = 0$, where ε_{4b}^0 and ε_{3t}^0 are the bottom energy of the fourth band and the top energy of the

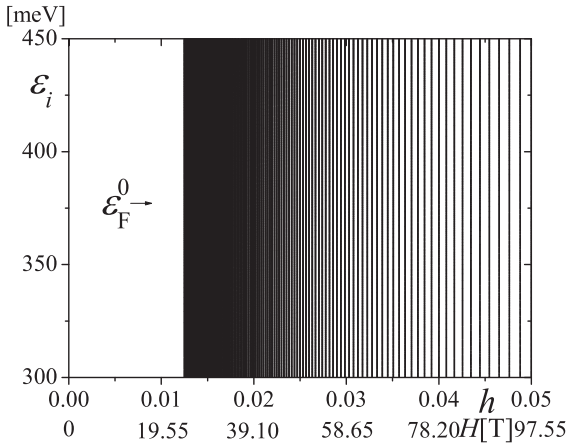

FIG. 6. Energy as a function of h for $V = 0$. [A close up figure of Fig. 5(a) at $h \approx 0$ and $\epsilon_i \approx \epsilon_F^0 \simeq 377.0$ meV, which is the Fermi energy at $h = 0$ for 3/4 filled case]. We take $h = 1/q$ with $20 \leqslant q \leqslant 80$ and $h = 2/(2m+1)$ with $20 \leqslant m \leqslant 79$, where the wave number $(k_x,k_y) = (n_x\pi/(30a),0)$ with $0 \leqslant n_x \leqslant 30$. The energy gaps cannot be seen in this scale.

third band, respectively (see Fig. 3). Note that the broadening of the Landau levels is not seen in the semiclassical theory [7] of the magnetic breakdown.

If we approximate electron and hole pockets in eigenvalues of Eq. (A11) as the anisotropic parabolic bands, it is expected that the Landau levels are semiclassically given by

$$\varepsilon_n^{\text{electron pocket}} \simeq \varepsilon_{4b}^0 + \frac{1}{C_{ep}}(n+\gamma)h \tag{8}$$

and

$$\varepsilon_n^{\text{hole pocket}} \simeq \varepsilon_{3t}^0 - \frac{1}{C_{hp}}(n+\gamma)h, \tag{9}$$

where $\gamma = 1/2$, C_{ep}, and C_{hp} are constants depending on the curvature of the anisotropic parabolic bands, respectively, and $n = 0,1,2,\ldots$. If this is the case, the ratio of the slope of the Landau levels as a function of the magnetic field should be

$$\left(0+\frac{1}{2}\right) : \left(1+\frac{1}{2}\right) : \left(2+\frac{1}{2}\right) : \cdots = 1:3:5:\cdots. \tag{10}$$

We obtain, however, that the ratio of the slope is approximately $1050 : 2100 : 3000 : \cdots \approx 1 : 2 : 3 : \cdots$, and $610 : 1500 : 2200 : \cdots \approx 2 : 5 : 7 : \cdots$ from the dotted lines in Fig. 7(a). When we approximate the slopes in the region of a weaker magnetic field as shown in Fig. 7 (c), we obtain the ratio of the slope as $1040 : 2570 : 3900 : \cdots \approx 2 : 5 : 8 : \cdots$ and $610 : 1550 : 2500 : \cdots \approx 2 : 5 : 8 : \cdots$. These results are inconsistent with the expected values of Eq. (10). As seen in Figs. 7(a) and 7(c) the fittings with the dotted lines are not good. Therefore the semiclassical quantization of Landau levels for free electron and free hole pockets is not a quantitatively acceptable approximation, even when we neglect the broadening of Landau levels.

Another interesting point in Fig. 7 is that there are many gaps with the same index (s_r,t_r) near 3/4-filling ($s_r = 3$). Gaps with the same index $(3,t_r)$ are closed or almost closed at

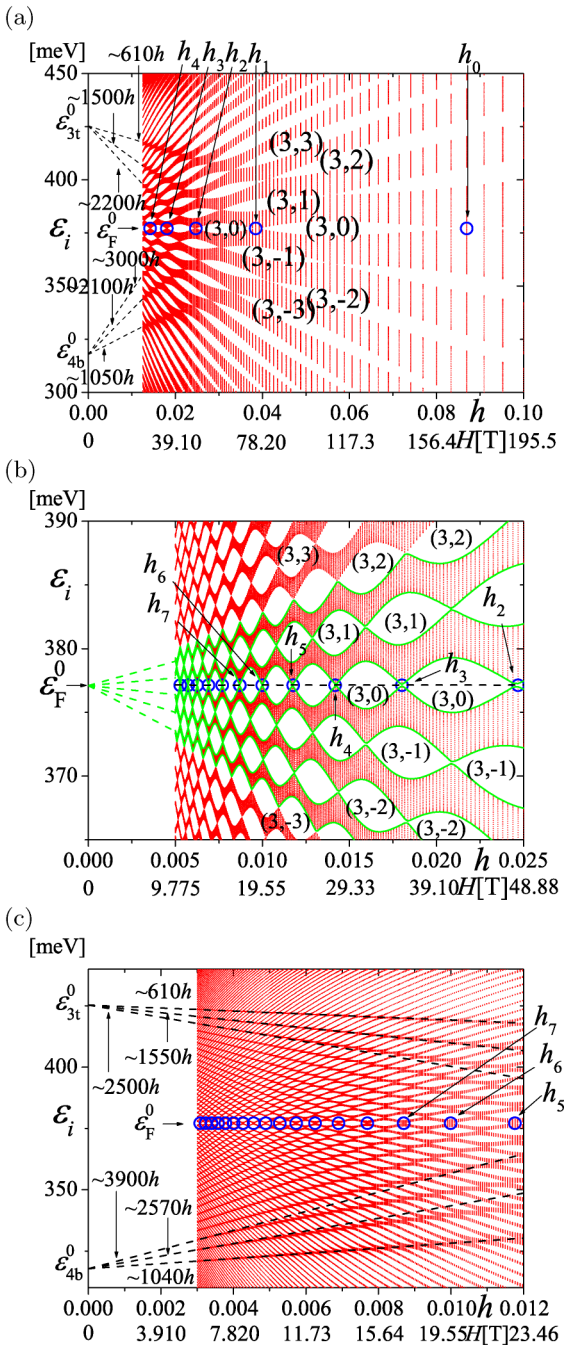

FIG. 7. (a) Energy as a function of h with the same parameters as those in Figs. 2(b), 3, and 5(b) ($V = 12.38$ meV), where $\varepsilon_F^0 \simeq 377.1$ meV. We take $h = 1/q$ with $10 \leqslant q \leqslant 80$ and $h = 2/(2m+1)$ with $10 \leqslant m \leqslant 79$. (b) An enlarged figure of (a). We take $h = 1/q$ with $40 \leqslant q \leqslant 200$ and $h = 2/(2m+1)$ with $40 \leqslant m \leqslant 199$. A dotted black line is the chemical potential as a function of h. (c) A figure for smaller h. The parameters are the same as those of (a) and (b). We take $h = 1/q$ with $84 \leqslant q \leqslant 333$ and $h = 2/(2m+1)$ with $84 \leqslant m \leqslant 332$. We take the wave number $(k_x,k_y) = (n_x\pi/(18a),0)$ with $0 \leqslant n_x \leqslant 18$ for $q > 200$, $(k_x,k_y) = (n_x\pi/(30a),0)$ with $0 \leqslant n_x \leqslant 30$ for $80 < q \leqslant 200$ and $(k_x,k_y) = (n_x\pi/(61a),0)$ with $0 \leqslant n_x \leqslant 61$ for $q \leqslant 80$.

points as a function of h. If the Landau levels [dotted lines in Figs. 7(a) and 7(c)], which were thought to be the quantized levels of electrons and holes in the electron and hole pockets,

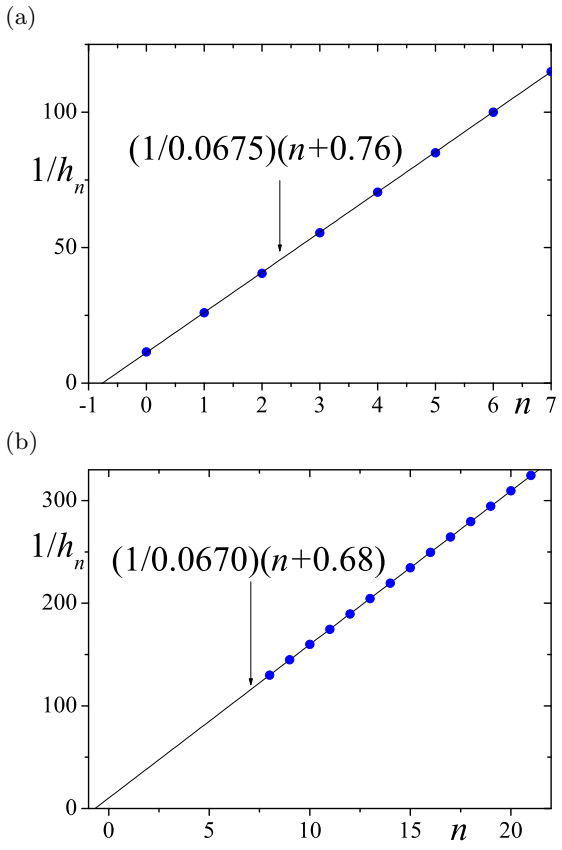

FIG. 8. $1/h_n$ as a function of n for (a) $0 \leqslant n \leqslant 7$ and (b) $8 \leqslant n \leqslant 21$. At the magnetic fields h_n ($n = 0,1,2,\ldots$), the energy gap with the index (3,0) is closed, as shown in Fig. 7.

were broadened in the tight-binding model, bands would be overlapped in finite ranges of h instead of closed at points. We can see the bands between the gaps $(3,t_r)$ and $(3,t_r+1)$ as if they start from the Fermi energy $\varepsilon_{\rm F}^0$ at $h = 0$, which are indicated by green lines in Fig. 7(b).

We draw blue circles in Fig. 7 at $\varepsilon_i = \varepsilon_{\rm F}^0$ and $h = h_0,h_1,h_2,h_3,\cdots$, at which the energy gap labeled by (3,0) is almost closed. We plot $1/h_n$ as a function of n in Fig. 8. We can fit $1/h_n$ as

$$\frac{1}{h_n} = \frac{1}{0.0675}(n+0.76) \quad (0 \leqslant n \leqslant 7), \tag{11}$$

$$\frac{1}{h_n} = \frac{1}{0.0670}(n+0.68) \quad (8 \leqslant n \leqslant 21), \tag{12}$$

in Fig. 8. In Eqs. (11) and (12), the regions of $1/h_n$ are $11.5 \leqslant 1/h_n \leqslant 115$ and $130 \leqslant 1/h_n \leqslant 324.5$, which correspond to $170 \geqslant H \geqslant 17$ T and 15.04 T $\geqslant H \geqslant 6.025$ T, respectively.

When we set $\varepsilon_n^{\text{electron pocket}} = \varepsilon_{\rm F}^0$ and $\varepsilon_n^{\text{hole pocket}} = \varepsilon_{\rm F}^0$ in Eqs. (8) and (9), we get

$$\frac{1}{h_n} \simeq \frac{1}{C_{\rm ep}\left(\varepsilon_{\rm F}^0 - \varepsilon_{\rm 4b}^0\right)}\left(n+\frac{1}{2}\right), \tag{13}$$

$$\frac{1}{h_n} \simeq \frac{1}{C_{\rm hp}\left(\varepsilon_{\rm 3t}^0 - \varepsilon_{\rm F}^0\right)}\left(n+\frac{1}{2}\right), \tag{14}$$

where $C_{\rm ep}(\varepsilon_{\rm F}^0 - \varepsilon_{\rm 4b}^0)$ and $C_{\rm hp}(\varepsilon_{\rm 3t}^0 - \varepsilon_{\rm F}^0)$ are given by the areas of the electron pocket and the hole pocket at $h = 0$ per the area of the Brillouin zone, respectively. The areas of electron pocket (black curves) and hole pocket (red curves) are the same and 0.0676 times the area of the Brillouin zone, as seen in Fig. 2(b). Thus the obtained values from the linear fitting (0.0675 and 0.0670) in Eqs. (11) and (12) are in good agreement with the semiclassical Landau quantization for parabolic bands, although γ deviates from $1/2$.

To analyze the closing of the gap in detail, we plot the close up figures near $h_4 = 2/141$ in Fig. 9. There are $564(=4\times q)$ bands when $h = p/q = 2/141$. When the band is 3/4 filled, the chemical potential is between the 423th and 424th bands, i.e., $r = 423$. The gap is almost closed at $k_x = \pm\pi/(4qa)$ but there is a small gap, which depends on k_y very slightly, as shown in Figs. 9(c) and 9(d).

Next, we study the energy for a larger $V = 37.14$ meV (Fig. 10). The width of the band at $V = 37.14$ meV is smaller than that at $V = 12.38$ meV, and it is smaller at smaller h. In this case the areas of the electron pocket and the hole pocket are smaller than those for $V = 12.38$ meV. The ratio of the slopes of the "Landau levels" starting from the bottom of the fourth band and the top of the third band [red dotted lines in Figs. 10(a) and 10(c)] becomes closer to that of free electrons, $1:3:5:\cdots$. This can be understood as follows. When V becomes large, the electron pocket and hole pocket are separated in the Brillouin zone and the areas of electron and hole pockets at $h = 0$ and 3/4-filling become small. Then we can safely adopt the approximation that electrons and holes in the pockets are treated as free electrons and free holes. The semiclassical picture of the magnetic breakdown between pockets may cause small effects. We plot the inverse of the magnetic fields h_n at which the gaps indexed by (3,0) are closed or almost closed, as a function of n in Fig. 11. This $1/h_n$ is fitted by a straight line with a larger slope than that of $V = 12.38$ meV (Fig. 8), which corresponds to the smaller areas of the electron and hole pockets. The phase factor γ obtained from the intersection with the n axis is near the free electron value, $1/2$.

We also study the case of $V = 86.5$ meV, when the top of the third band $\varepsilon_{\rm 3t}$ and the bottom of the fourth band $\varepsilon_{\rm 4b}$ are the same and the electron and hole pockets disappear at 3/4-filling, as shown in Fig. 4. We plot the energy as a function of h in Fig. 12. The bandwidths are very narrow. Since the ratio of the slopes of the Landau levels is close to $1:3:5:\cdots$, the bands are recognized as Landau levels for free electrons and holes.

If the holes or the electrons are doped, the chemical potential is above or below the dotted blue line in Fig. 7(b) ($V = 12.38$ meV) or the dotted orange line in Fig. 10(b) ($V = 37.14$ meV). The Hall conductance is quantized when the chemical potential is in the energy gap, but it is not quantized when the chemical potential is within the broadened band. For a reasonable value of anion potential ($V = 12.38$ meV), the energy band is broadened. Therefore the Hall conductance is quantized only in some regions of the magnetic field, if electrons or hales are doped, and it is not quantized in other regions of the magnetic field.

VI. MAGNETIZATION AND DE HAAS–VAN ALPHEN OSCILLATIONS

The oscillatory part of the magnetization with the fixed chemical potential (μ) at the temperature (T) is given by the

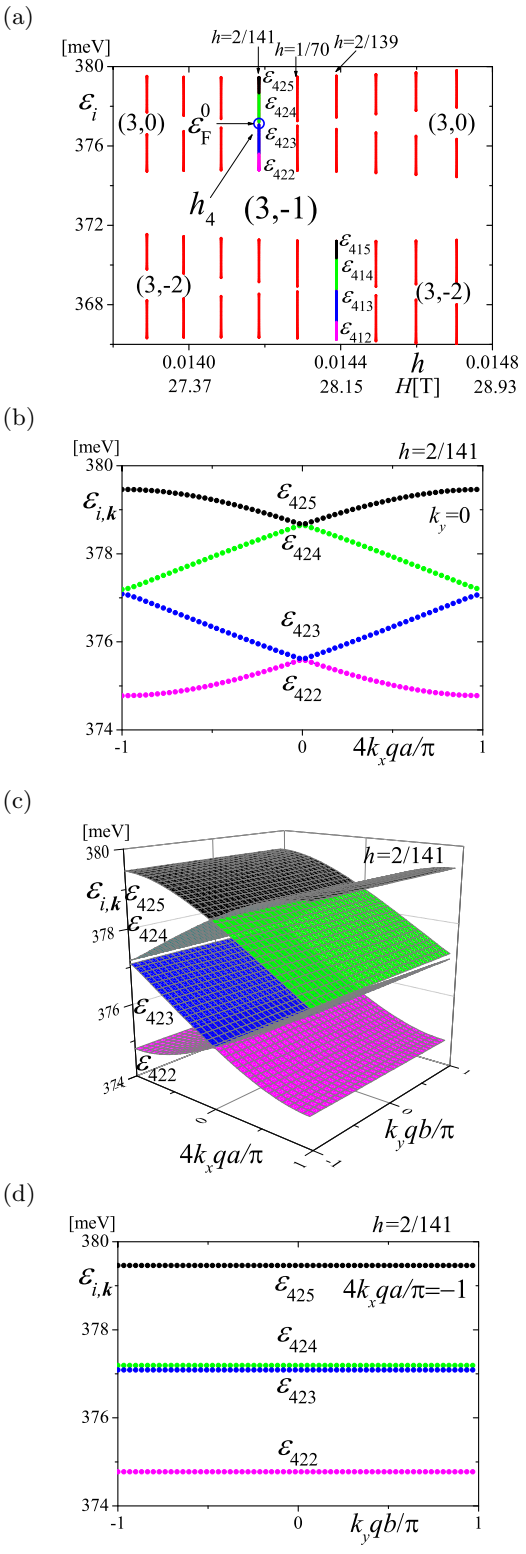

FIG. 9. (a) A close up figure of Fig. 7 near h_4 ($V = 12.38$ meV). We take $h = 1/72$, $2/143$, $1/71$, $2/141$, $1/70$, $2/139$, $1/69$, $2/137$, and $1/68$. (b) Energies as a function of k_x at $h = 2/141$ and $k_y = 0$. (c) 3D plot of the energies at $h = 2/141$. (d) There is a small gap between ε_{423} and ε_{424} at $k_x = \pm\pi/(4qa)$. The gap is almost independent of k_y.

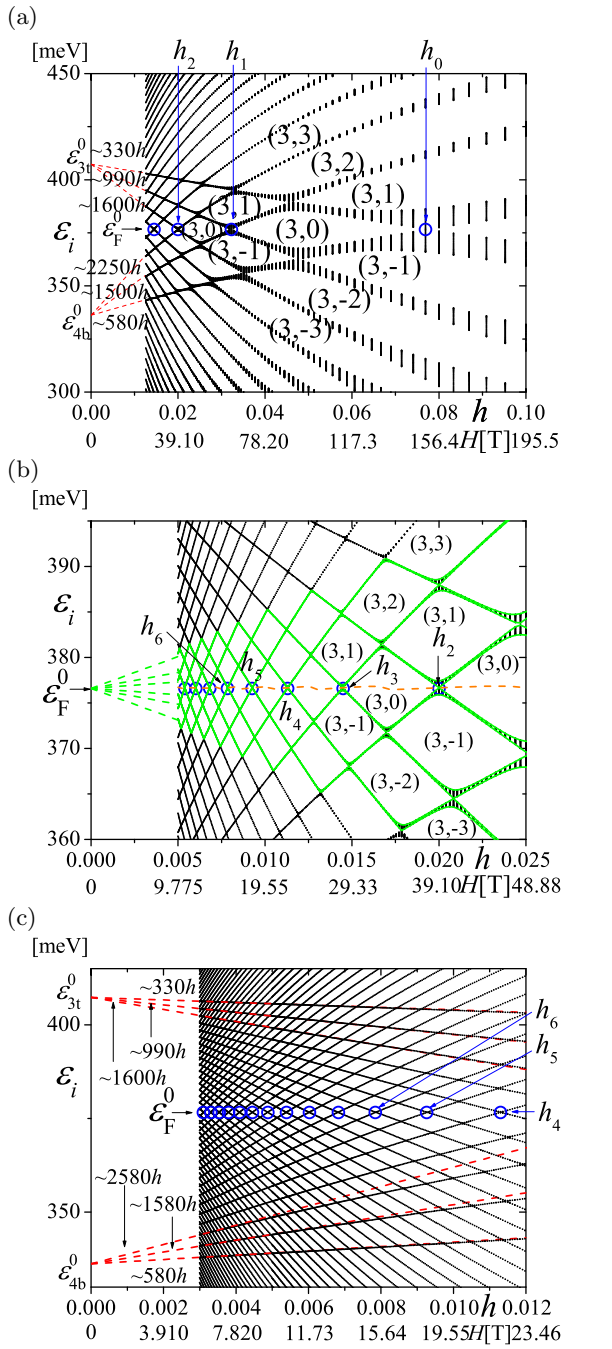

FIG. 10. (a) Energy as a function of h for $V = 37.14$ meV. Other parameters are the same as those in Fig. 2(b). The direct band gap at $h = 0$ is $2\Delta \simeq 53.32$ meV, the Fermi energy for the $3/4$ filled case is $\varepsilon_{\rm F}^0 \simeq 376.6$ meV, the top energy of the third band is $\varepsilon_{\rm 3t}^0 \simeq 407.3$ meV, and the bottom energy of the forth band is $\varepsilon_{\rm 4b}^0 \simeq 336.2$ meV. (b) An enlarged figure of (a). A dotted orange line is the chemical potential as a function of h. (c) A figure for smaller h. The parameters are the same as those of (a) and (b). In all figures, the values of q and the wave number (k_x,k_y) are the same as those of Fig. 7. Small blue circles indicate the magnetic fields $h_0, h_1, h_2, \cdots$ at which the gaps indexed by (3,0) are closed or almost closed.

LK formula [6,12–20]. In the generalized LK formula in two-dimensional metals the magnetization oscillates periodically as a function $1/H$ with the period

$$f = \frac{c\hbar A}{2\pi e}, \tag{15}$$

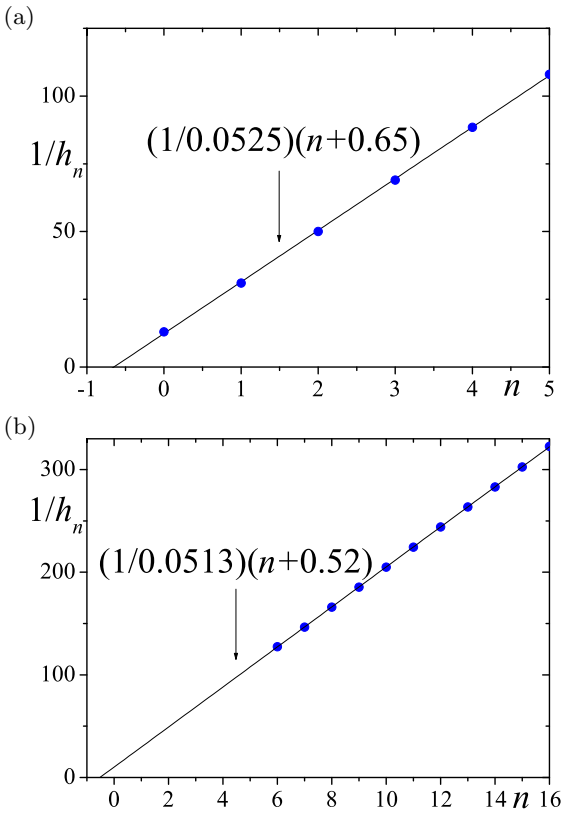

FIG. 11. Similar plot as Fig. 8 for $V = 37.14$ meV.

where A is the area of the Fermi surface at $H = 0$. The generalized LK formula at $T = 0$ for the two-dimensional metals is given by

$$M^{\mathrm{LK}} = -\frac{e}{2\pi^2 c\hbar}\frac{A}{\frac{\partial A}{\partial \mu}}\sum_{l=1}^{\infty}\frac{1}{l}\sin\left[2\pi l\left(\frac{f}{H}-\gamma\right)\right]. \quad (16)$$

Note that the oscillation part of the magnetization in LK formula is zero at

$$H = H_n \quad (17)$$

and we obtain

$$\frac{1}{H_n} = \frac{1}{f}(n+\gamma) \quad (18)$$

with $n = 0,1,2,\ldots$. Namely, $M^{\mathrm{LK}} = 0$ appears periodically as a function of $1/H$ with the frequency, f. The amplitude of the oscillation at $T = 0$ is independent of H in the LK formula. In the LK formula, the broadening of the Landau levels in the tight-binding model is not taken into account.

In this section, we study dHvA oscillation in $(TMTSF)_2NO_3$ by taking the effects of the magnetic field in the tight-binding model. The energy $\varepsilon_{i,\mathbf{k}}$ in the magnetic field is obtained as the eigenvalues of $4q \times 4q$ matrix $\tilde{\varepsilon}_{\mathbf{k}}$ given in Eq. (B23), where $i = 1 \sim 4q$. The thermodynamic potential Ω per sites at T is obtained as

$$\Omega = -\frac{k_B T}{4qN_k}\sum_{i=1}^{4q}\sum_{\mathbf{k}}\ln\left[\exp\left(\frac{\mu-\varepsilon_{i,\mathbf{k}}}{k_B T}\right)+1\right], \quad (19)$$

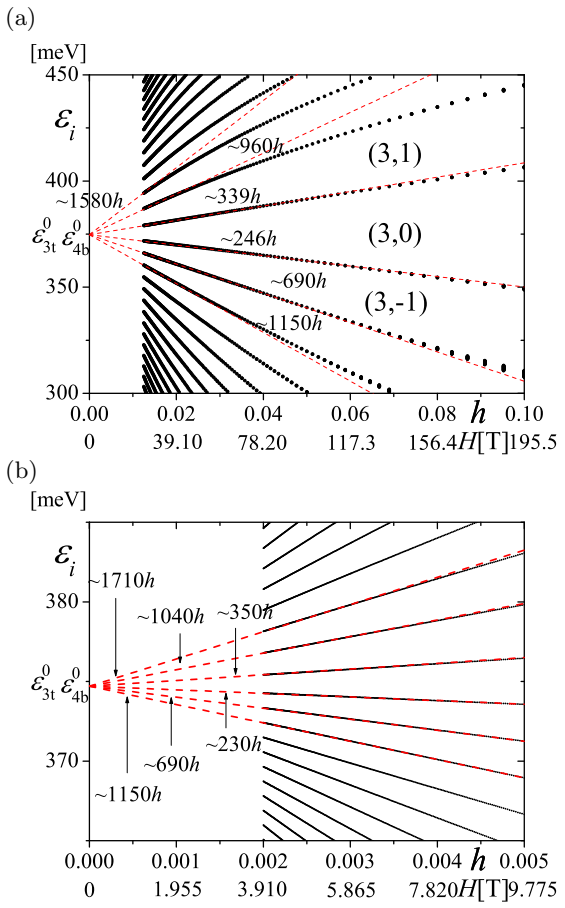

FIG. 12. (a) Energy as a function of h at $V = 86.5$ meV, where $2\Delta \simeq 123.2$ meV, $\varepsilon^0_{\mathrm{F}} = \varepsilon^0_{3t} = \varepsilon^0_{4b} \simeq 374.7$ meV. We take $h = 1/q$ with $10 \leqslant q \leqslant 80$ and $h = 2/q$ with $q = 2m+1$ and $20 \leqslant m \leqslant 59$, where the wave number $(k_x,k_y) = (n_x\pi/(30a),0)$ with $0 \leqslant n_x \leqslant 30$. (b) An enlarged figure of (a). We take $h = 1/q$ with $200 \leqslant q \leqslant 500$, where $(k_x,k_y) = (n_x\pi/(18a),0)$ with $0 \leqslant n_x \leqslant 18$.

where k_B is the Boltzmann constant and N_k is the number of $\mathbf{k}$ points taken in the magnetic Brillouin zone. At $T = 0$, Ω becomes the total energy with fixed μ,

$$E_\mu = \frac{1}{4qN_k}\sum_{\varepsilon_{i,\mathbf{k}}\leqslant\mu}(\varepsilon_{i,\mathbf{k}}-\mu). \quad (20)$$

The magnetization is obtained in grand canonical ensemble by

$$M_\mu = -\frac{\partial\Omega}{\partial h}. \quad (21)$$

On the other hand, when the electron number is fixed [in $(TMTSF)_2X$, electrons are ν-filling with $\nu = 3/4$], the magnetic-field dependence of the chemical potential is not negligible in two-dimensional systems in general [6,12–15], whereas it can be neglected in three-dimensional metals. In this study, the Helmholtz free energy and the magnetization are calculated in the canonical ensemble with the fixed electron number. In that case, the chemical potential, μ, should be obtained by the equation

$$\nu = \frac{1}{4qN_k}\sum_{i=1}^{4q}\sum_{\mathbf{k}}\frac{1}{\exp\left(\frac{\varepsilon_{i,\mathbf{k}}-\mu}{k_B T}\right)+1}. \quad (22)$$

The Helmholtz free energy (F) per sites at T is given by

$$F = -\frac{k_B T}{4qN_k}\sum_{i=1}^{4q}\sum_{\mathbf{k}} \ln\left[\exp\left(\frac{\mu-\varepsilon_{i,\mathbf{k}}}{k_B T}\right)+1\right]+\mu\nu. \tag{23}$$

At $T=0$, it becomes

$$E_\nu = \frac{1}{4qN_k}\sum_{\varepsilon_{i,\mathbf{k}}\leqslant\mu}\varepsilon_{i,\mathbf{k}}. \tag{24}$$

The magnetization for fixed electron filling ν is given by

$$M_\nu = -\frac{\partial F}{\partial h}. \tag{25}$$

We obtain the magnetization by the numerical differentiation.

As seen in Figs. 7(b) and 10(b), the chemical potentials (dotted black and orange lines) for $\nu = 3/4$ are in the gap labeled by (3,0) and almost independent of h. Therefore, in both cases of $V = 12.38$ and 37.14 meV, M_μ and M_ν are expected to be almost the same. Indeed, we obtained a negligible difference between M_μ and M_ν in the numerical calculation. In Figs. 13(a) and 13(b) and Figs. 14(a) and 14(b), we plot F and M_ν as a function h with $V = 12.38$ meV and 37.14 meV, respectively. The periodical oscillations as a function of $1/h$ are seen in Figs. 13(c) and 14(c), respectively. These oscillations are thought to correspond to the dHvA oscillation for electrons and holes in semiclassical theory. The free energy, F, has local maximum values at $h = h_n$, which are shown as blue circles in Figs. 7 and 10. At $h = h_n$, the gaps labeled by (3,0) are closed or almost closed. The free energy may be lowered by opening a finite gap at the Fermi energy. Therefore it is reasonable that the free energy is a local maximum at $h = h_n$. As a result, the magnetization is zero at $h = h_n$. Since $1/h_n$ is fitted by a straight line (see Figs. 8 and 11) proportional to $(n+\gamma)$, the magnetization oscillates periodically as a function $1/h$ (dHvA oscillation). These frequencies (0.0675 and 0.0670) in Fig. 8 are almost the same as the areas of the electron and hole pockets in Fig. 2(b) per area of the Brillouin zone. It is expected that, in the dHvA experiment of $(TMTSF)_2NO_3$, $\gamma = 0.76$ in Eq. (11) [$\gamma = 0.68$ in Eq. (12)] are estimated at $17 \leqslant H \leqslant 170$ T ($6.025\ \text{T} \leqslant H \leqslant 15.04$ T). From the experiment of SdH oscillations [59], γ is estimated to be 0. The SdH experiment was performed in the SDW state. The amplitude of the SDW order parameter may depend on the magnetic field. Therefore it is not easy to compare the experiment with our result calculated in the metallic state without SDW order.

For larger V ($V = 37.14$ meV), the amplitude of the magnetization oscillations is almost constant for $1/h \gtrsim 100$ (i.e., $H \lesssim 19.55$ T) at $T = 0$ as shown in Figs. 14(b) and 14(c). The almost constant field dependence of the amplitude and the sawtooth shape of M_ν [Fig. 14(c)] are the same as those of M^{LK} [Eq. (16)] for the fixed chemical potential case in two-dimensional metals. For the realistic value of V ($V = 12.38$ meV), the sawtooth shape is similar. However, the amplitude of the magnetization oscillations increases as a function of $1/h$ for $1/h \lesssim 333$ ($H \gtrsim 5.865$ T) at $T = 0$ as shown in Figs. 13(b) and 13(c). The h dependence of the amplitude of the magnetization oscillation is caused by the broadening of Landau levels.

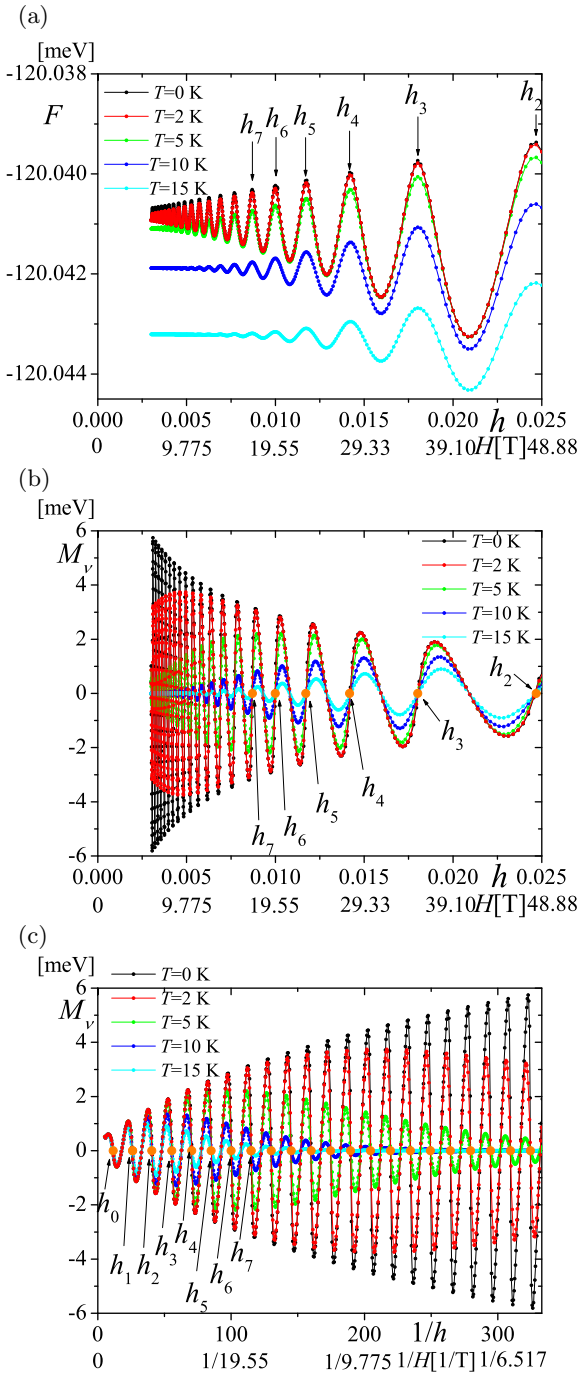

FIG. 13. Free energy (a) and magnetizations as a function of h (b) and as a function of $1/h$ (c) at $V = 12.38$ meV for $T = 0,5,10$ and 15 K. We take $h = 1/q$ with $5 \leqslant q \leqslant 333$ and $h = 2/q$ with $q = 2m+1$ and $5 \leqslant m \leqslant 332$, where $(k_x,k_y) = (n_x\pi/(6a),0)$ with $0 \leqslant n_x \leqslant 6$ for $q > 333$, $(k_x,k_y) = (n_x\pi/(13a),0)$ with $0 \leqslant n_x \leqslant 13$ for $200 < q \leqslant 333$, $(k_x,k_y) = (n_x\pi/(30a),0)$ with $0 \leqslant n_x \leqslant 30$ for $80 < q \leqslant 200$ and $(k_x,k_y) = (n_x\pi/(61a),0)$ with $0 \leqslant n_x \leqslant 61$ for $q \leqslant 80$.

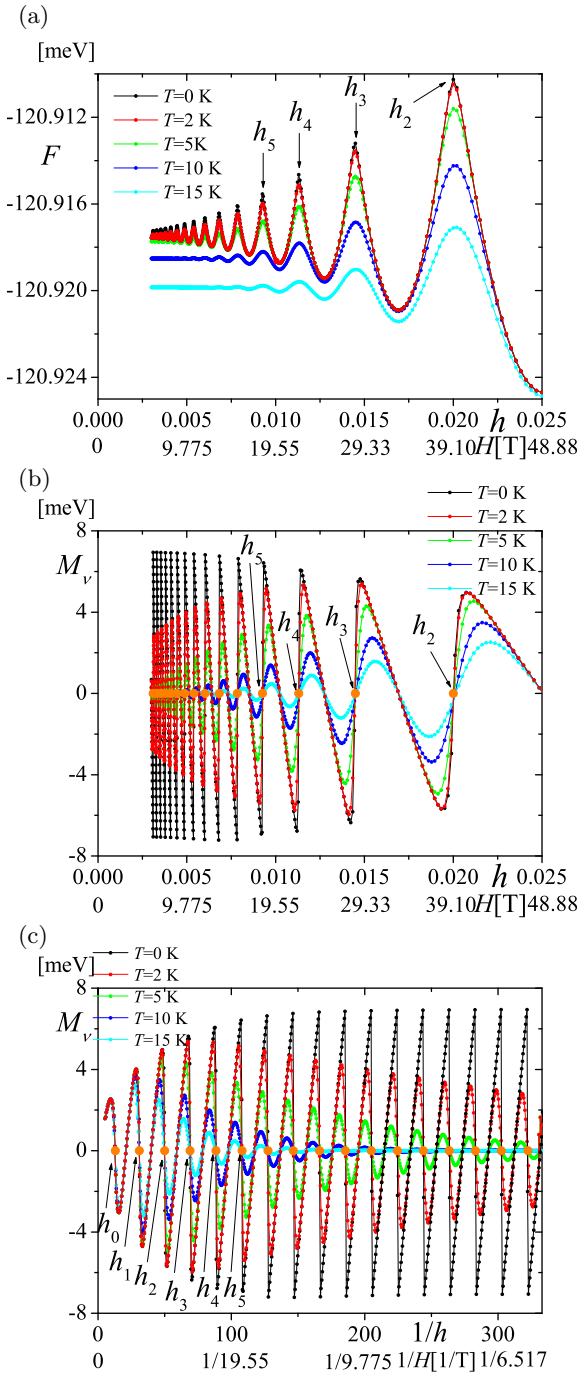

FIG. 14. Free energy (a) and magnetizations as a function of h (b) and as a function of $1/h$ (c) at $V = 37.14$ meV for $T = 0$, 5, 10, and 15 K. We take the same values for q and (k_x, k_y) as those of Fig. 13.

VII. CONCLUSIONS

We use the spinless tight-binding model on a two-dimensional rectangular lattice for $(TMTFS)_2NO_3$ with realistic band parameters and potentials due to the effect of the anion ordering. The effects of a uniform magnetic field $\sim$6 T are treated by introducing phase factors for the electron hoppings. We think this quantum-mechanical treatment of the uniform magnetic field provides us more appropriate results than the semiclassical theory [7,8], in which a Landau quantization of the semiclassical closed orbits of electrons and holes is assumed by the magnetic breakdown phenomenon with a phenomenological parameter.

For a reasonable value of the anion potential ($V = 12.38$ meV), the energy bands in the magnetic field are broadened (Fig. 7), which is caused by the tight-binding nature of electrons. In principle, several much smaller gaps should exist in the broadened Landau levels, but they are very small and may not be seen in experiments at finite temperatures. If the electrons or the holes are doped, the region of the nonquantized Hall effect becomes wider as the magnetic field increases due to the broadening of Landau levels. This broadening causes an interesting phenomenon that the amplitude of de Haas–van Alphen oscillations at $T = 0$ decreases as the magnetic field increases. This is different from the LK formula although the chemical potential is almost constant in this calculation.

For a larger value of the anion potential ($V = 37.14$ meV), the energy bands in the magnetic field are narrow and are seen as slightly broadened Landau levels (Fig. 10), which is similar to the energy obtained from the semiclassical theory [7]. In this case, the amplitude of de Haas–van Alphen oscillation at $T = 0$ is almost independent of the magnetic field at low field, as in the semiclassical LK formula [6,12–20]. The energy gaps at 3/4-filling are closed or almost closed periodically at the inverse magnetic field, which was seen in both cases of $V = 12.38$ and 37.14 meV.

We would like to emphasize the difference between the quantum-mechanical theory and semiclassical theory [7] for $(TMTSF)_2NO_3$, which has electron and hole pockets at $h = 0$. Unlike the cases in the semiclassical theory, we have shown that the Landau levels are sufficiently broadened near the Fermi energy and the energy gaps are closed or almost closed periodically as a function of the inverse magnetic field. Since we have neglected the hoppings between the conducting plane, we have not discussed the effects of the direction of the magnetic field. We have not studied the transport properties in this paper, either. Therefore the angular-dependent magnetoresistance have to be studied quantum mechanically in the future.

It is possible to observe the results shown about the quantum Hall conductance and dHvA oscillation in $(TMTSF)_2NO_3$ without SDW (for example, at $T_{SDW} < T < T_{AO}$, where SDW state does not exist). The wider region of the nonquantized Hall effect upon increasing the magnetic field will be observed under doping when the broadening of Landau levels is larger than thermal broadening. The Hall conductance [60] and magnetization [61] have been observed experimentally in $(TMTSF)_2NO_3$ in the SDW state, but not in the metallic state. If the SDW state is suppressed by pressure, which affects the tight-binding parameters slightly but changes the nesting of the Fermi surface drastically, the magnetic field dependence of the amplitude of dHvA oscillation will be observed at low temperature.

ACKNOWLEDGMENT

One of the authors (K.K.) thanks Noriaki Matsunaga for useful discussions and information of experiments.

APPENDIX A: ENERGY AT $H = 0$

We use the spinless two-dimensional tight-binding model on a rectangular lattice in the unit cell with four sites (A, B, A', and B'), where TMTSF molecules correspond to sites. The effect of the anion ordering is represented by the on-site potential along x axis, (V, V, $-V$, $-V$), as shown in Figs. 1(b) and 1(c). We show the Fermi surface in Figs. 2(a) and 2(b) for $V = 0$ and 12.38 meV, respectively.

The Bravais lattices for a rectangular lattice are given by

$$\mathbf{v}_1 = (4a,0) \tag{A1}$$

and

$$\mathbf{v}_2 = (0,b), \tag{A2}$$

where a and b are the lattice spacings of TMTSF molecules. In this model, the Hamiltonian is given by

$$\begin{aligned}\hat{\mathcal{H}}_0 &= \sum_{i,j} t_{ij} c_i^\dagger c_j + \sum_i V_i c_i^\dagger c_i \\ &= \sum_{\mathbf{r}_j} \Big[t_{\mathrm{S1}} \big(a_{\mathbf{r}_j}^\dagger b_{\mathbf{r}_j} + a_{\mathbf{r}_j}'^\dagger b_{\mathbf{r}_j}' + b_{\mathbf{r}_j}^\dagger a_{\mathbf{r}_j} + b_{\mathbf{r}_j}'^\dagger a'_{\mathbf{r}_j} \big) + t_{\mathrm{S2}} \big(b_{\mathbf{r}_j}^\dagger a_{\mathbf{r}_j}' + b_{\mathbf{r}_j}'^\dagger a_{\mathbf{r}_j+\mathbf{v}_1} + a_{\mathbf{r}_j}'^\dagger b_{\mathbf{r}_j} + a_{\mathbf{r}_j+\mathbf{v}_1}^\dagger b_{\mathbf{r}_j}' \big) \\ &\quad + t_{\mathrm{I1}} \big(a_{\mathbf{r}_j+\mathbf{v}_2}^\dagger b_{\mathbf{r}_j} + a_{\mathbf{r}_j+\mathbf{v}_2}'^\dagger b_{\mathbf{r}_j}' + b_{\mathbf{r}_j}^\dagger a_{\mathbf{r}_j+\mathbf{v}_2} + b_{\mathbf{r}_j}'^\dagger a_{\mathbf{r}_j+\mathbf{v}_2}' \big) + t_{\mathrm{I2}} \big(b_{\mathbf{r}_j+\mathbf{v}_2}^\dagger a_{\mathbf{r}_j}' + a_{\mathbf{r}_j}'^\dagger b_{\mathbf{r}_j+\mathbf{v}_2} + b_{\mathbf{r}_j+\mathbf{v}_2}'^\dagger a_{\mathbf{r}_j+\mathbf{v}_1} + a_{\mathbf{r}_j+\mathbf{v}_1}^\dagger b_{\mathbf{r}_j+\mathbf{v}_2}' \big) \\ &\quad + t_{\mathrm{I3}} \big(a_{\mathbf{r}_j}^\dagger a_{\mathbf{r}_j+\mathbf{v}_2} + a_{\mathbf{r}_j}'^\dagger a_{\mathbf{r}_j+\mathbf{v}_2}' + b_{\mathbf{r}_j}^\dagger b_{\mathbf{r}_j+\mathbf{v}_2} + b_{\mathbf{r}_j}'^\dagger b_{\mathbf{r}_j+\mathbf{v}_2}' + a_{\mathbf{r}_j+\mathbf{v}_2}^\dagger a_{\mathbf{r}_j} + a_{\mathbf{r}_j+\mathbf{v}_2}'^\dagger a_{\mathbf{r}_j}' + b_{\mathbf{r}_j+\mathbf{v}_2}^\dagger b_{\mathbf{r}_j} + b_{\mathbf{r}_j+\mathbf{v}_2}'^\dagger b_{\mathbf{r}_j}' \big) \\ &\quad + t_{\mathrm{I4}} \big(a_{\mathbf{r}_j+\mathbf{v}_2}^\dagger a_{\mathbf{r}_j}' + b_{\mathbf{r}_j+\mathbf{v}_2}^\dagger b_{\mathbf{r}_j}' + a_{\mathbf{r}_j+\mathbf{v}_2}'^\dagger a_{\mathbf{r}_j+\mathbf{v}_1} + b_{\mathbf{r}_j+\mathbf{v}_2}'^\dagger b_{\mathbf{r}_j+\mathbf{v}_1} + a_{\mathbf{r}_j}'^\dagger a_{\mathbf{r}_j+\mathbf{v}_2} + b_{\mathbf{r}_j}'^\dagger b_{\mathbf{r}_j+\mathbf{v}_2} + a_{\mathbf{r}_j+\mathbf{v}_1}^\dagger a_{\mathbf{r}_j+\mathbf{v}_2}' + b_{\mathbf{r}_j+\mathbf{v}_1}^\dagger b_{\mathbf{r}_j+\mathbf{v}_2}' \big) \\ &\quad + V \big(a_{\mathbf{r}_j}^\dagger a_{\mathbf{r}_j} + b_{\mathbf{r}_j}^\dagger b_{\mathbf{r}_j} - a_{\mathbf{r}_j}'^\dagger a_{\mathbf{r}_j}' - b_{\mathbf{r}_j}'^\dagger b_{\mathbf{r}_j}' \big) \Big], \end{aligned} \tag{A3}$$

where $a_{\mathbf{r}_j}^\dagger$, $b_{\mathbf{r}_j}^\dagger$, $a_{\mathbf{r}_j}'^\dagger$ and $b_{\mathbf{r}_j}'^\dagger$ ($a_{\mathbf{r}_j}$, $b_{\mathbf{r}_j}$, $a'_{\mathbf{r}_j}$ and $b'_{\mathbf{r}_j}$) are creation (annihilation) operators for A, B, A', and B' sites in jth unit cell, respectively. By using the following Fourier transform:

$$a_{\mathbf{r}_j} = \sum_{\mathbf{k}} e^{i\mathbf{k}\cdot\mathbf{r}_j} a_{\mathbf{k}}, \tag{A4}$$

$$b_{\mathbf{r}_j} = \sum_{\mathbf{k}} e^{i\mathbf{k}\cdot(\mathbf{r}_j+\frac{1}{4}\mathbf{v}_1)} b_{\mathbf{k}}, \tag{A5}$$

$$a'_{\mathbf{r}_j} = \sum_{\mathbf{k}} e^{i\mathbf{k}\cdot(\mathbf{r}_j+\frac{1}{2}\mathbf{v}_1)} a'_{\mathbf{k}}, \tag{A6}$$

$$b'_{\mathbf{r}_j} = \sum_{\mathbf{k}} e^{i\mathbf{k}\cdot(\mathbf{r}_j+\frac{3}{4}\mathbf{v}_1)} b'_{\mathbf{k}}, \tag{A7}$$

we obtain the Hamiltonian in the momentum space as

$$\hat{\mathcal{H}}_0 = \sum_{\mathbf{k}} C_{\mathbf{k}}^\dagger \varepsilon_{\mathbf{k}} C_{\mathbf{k}}, \tag{A8}$$

where

$$C_{\mathbf{k}}^\dagger = (a_{\mathbf{k}}^\dagger, b_{\mathbf{k}}^\dagger, a_{\mathbf{k}}'^\dagger, b_{\mathbf{k}}'^\dagger) \tag{A9}$$

and

$$C_{\mathbf{k}} = \begin{pmatrix} a_{\mathbf{k}} \\ b_{\mathbf{k}} \\ a_{\mathbf{k}}'^\dagger \\ b_{\mathbf{k}}'^\dagger \end{pmatrix}. \tag{A10}$$

In this equation, $\varepsilon_{\mathbf{k}}$ is a 4×4 matrix as follows:

$$\varepsilon_{\mathbf{k}} = \begin{pmatrix} \epsilon_{\mathbf{k}AA} & \epsilon_{\mathbf{k}AB} & \epsilon_{\mathbf{k}AA'} & \epsilon_{\mathbf{k}AB'} \\ \epsilon_{\mathbf{k}BA} & \epsilon_{\mathbf{k}BB} & \epsilon_{\mathbf{k}BA'} & \epsilon_{\mathbf{k}BB'} \\ \epsilon_{\mathbf{k}A'A} & \epsilon_{\mathbf{k}A'B} & \epsilon_{\mathbf{k}A'A'} & \epsilon_{\mathbf{k}A'B'} \\ \epsilon_{\mathbf{k}B'A} & \epsilon_{\mathbf{k}B'B} & \epsilon_{\mathbf{k}B'A'} & \epsilon_{\mathbf{k}B'B'} \end{pmatrix} \tag{A11}$$

with

$$\epsilon_{\mathbf{k}AA} = \epsilon_{\mathbf{k}BB} = 2t_{\mathrm{I3}} \cos(bk_y) + V, \tag{A12}$$

$$\epsilon_{\mathbf{k}A'A'} = \epsilon_{\mathbf{k}B'B'} = 2t_{\mathrm{I3}} \cos(bk_y) - V, \tag{A13}$$

$$\epsilon_{\mathbf{k}AB} = \epsilon_{\mathbf{k}A'B'} = t_{\mathrm{S1}} e^{iak_x} + t_{\mathrm{I1}} e^{i(ak_x - bk_y)}, \tag{A14}$$

$$\epsilon_{\mathbf{k}BA'} = \epsilon_{\mathbf{k}B'A} = t_{\mathrm{S2}} e^{iak_x} + t_{\mathrm{I2}} e^{i(ak_x - bk_y)}, \tag{A15}$$

$$\epsilon_{\mathbf{k}BA} = \epsilon_{\mathbf{k}B'A'} = \epsilon_{\mathbf{k}AB}^*, \tag{A16}$$

$$\epsilon_{\mathbf{k}AB'} = \epsilon_{\mathbf{k}A'B} = \epsilon_{\mathbf{k}BA'}^*, \tag{A17}$$

$$\epsilon_{\mathbf{k}AA'} = \epsilon_{\mathbf{k}BB'} = 2t_{\mathrm{I4}} \cos(2ak_x - bk_y), \tag{A18}$$

$$\epsilon_{\mathbf{k}A'A} = \epsilon_{\mathbf{k}B'B} = \epsilon_{\mathbf{k}AA'}. \tag{A19}$$

When $V = 0$, the Hamiltonian matrix of $\hat{\mathcal{H}}_0$ can be reduced to the 2×2 as

$$\varepsilon_{\mathbf{k}}^0 = \begin{pmatrix} \epsilon_{\mathbf{k}AA}^{(0)} & \epsilon_{\mathbf{k}AB}^{(0)} \\ \epsilon_{\mathbf{k}BA}^{(0)} & \epsilon_{\mathbf{k}BB}^{(0)} \end{pmatrix} \tag{A20}$$

with

$$\begin{aligned}\epsilon_{\mathbf{k}AA}^{(0)} &= \epsilon_{\mathbf{k}BB}^{(0)} \\ &= 2t_{\mathrm{I3}} \cos(bk_y) + 2t_{\mathrm{I4}} \cos(2ak_x - bk_y), \end{aligned} \tag{A21}$$

$$\epsilon_{\mathbf{k}AB}^{(0)} = t_{\mathrm{S1}} e^{iak_x} + t_{\mathrm{S2}} e^{-iak_x} + t_{\mathrm{I1}} e^{i(ak_x - bk_y)} + t_{\mathrm{I2}} e^{-i(ak_x - bk_y)}, \tag{A22}$$

$$\epsilon_{\mathbf{k}BA}^{(0)} = \big(\epsilon_{\mathbf{k}AB}^{(0)}\big)^*. \tag{A23}$$

APPENDIX B: ENERGY IN THE MAGNETIC FIELD

The Hamiltonian in a spinless two-dimensional tight-binding model in the magnetic field becomes

$$\hat{\mathcal{H}} = \sum_{i,j} t_{ij} c_i^\dagger c_j e^{i2\pi\phi_{ij}} + \sum_i V_i c_i^\dagger c_i, \tag{B1}$$

where c_i is a_{r_i}, b_{r_i}, a'_{r_i}, or b'_{r_i}, and the phase factor (ϕ_{ij}) is given by

$$\phi_{ij} = \frac{e}{ch} \int_{\mathbf{r}_i}^{\mathbf{r}_j} \mathbf{A} \cdot d\mathbf{l}, \tag{B2}$$

In this study, the magnetic field is applied perpendicular to the x-y plane and we take the Landau gauge $\mathbf{A} = (0, Hx, 0)$. The flux thorough the unit cell ($4ab$) is

$$\Phi = 4abH. \tag{B3}$$

The phase factors are given as

$$\phi^{(n)}_{\mathrm{I}1AB} = -\phi^{(n)}_{\mathrm{I}1BA} = \frac{\Phi}{\phi_0}\left(n + \frac{1}{8}\right), \tag{B4}$$

$$\phi^{(n)}_{\mathrm{I}1A'B'} = -\phi^{(n)}_{\mathrm{I}1B'A'} = \frac{\Phi}{\phi_0}\left(n + \frac{5}{8}\right), \tag{B5}$$

$$\phi^{(n)}_{\mathrm{I}2BA'} = -\phi^{(n)}_{\mathrm{I}2A'B} = \frac{\Phi}{\phi_0}\left(n + \frac{3}{8}\right), \tag{B6}$$

$$\phi'^{(n-1,n)}_{\mathrm{I}2B'A} = \frac{\Phi}{\phi_0}\left(n - \frac{1}{8}\right), \tag{B7}$$

$$\phi'^{(n+1,n)}_{\mathrm{I}2AB'} = -\frac{\Phi}{\phi_0}\left(n + \frac{7}{8}\right), \tag{B8}$$

$$\phi^{(n)}_{\mathrm{I}3AA} = \frac{\Phi}{\phi_0} n, \tag{B9}$$

$$\phi^{(n)}_{\mathrm{I}3BB} = \frac{\Phi}{\phi_0}\left(n + \frac{1}{4}\right), \tag{B10}$$

$$\phi^{(n)}_{\mathrm{I}3A'A'} = \frac{\Phi}{\phi_0}\left(n + \frac{1}{2}\right), \tag{B11}$$

$$\phi^{(n)}_{\mathrm{I}3B'B'} = \frac{\Phi}{\phi_0}\left(n + \frac{3}{4}\right), \tag{B12}$$

$$\phi^{(n)}_{\mathrm{I}4AA'} = -\phi^{(n)}_{\mathrm{I}4A'A} = \frac{\Phi}{\phi_0}\left(n + \frac{1}{4}\right), \tag{B13}$$

$$\phi^{(n)}_{\mathrm{I}4BB'} = -\phi^{(n)}_{\mathrm{I}4B'B} = \frac{\Phi}{\phi_0}\left(n + \frac{1}{2}\right), \tag{B14}$$

$$\phi'^{(n-1,n)}_{\mathrm{I}4A'A} = \frac{\Phi}{\phi_0}\left(n - \frac{1}{4}\right), \tag{B15}$$

$$\phi'^{(n-1,n)}_{\mathrm{I}4B'B} = \frac{\Phi}{\phi_0} n, \tag{B16}$$

and the phase factor is zero for hoppings $t_{\mathrm{S}1}$ and $t_{\mathrm{S}2}$. The phase factor $\phi^{(n)}_{\mu\alpha\beta}$ ($\mu = $ I1,I2,I3 or I4, α and β are A, B, A', or B') is the phase factor for the hopping μ from the site β to the site α both in the nth unit cell ($4na \leqslant x_i < 4(n+1)a$ for both α and β). When $\alpha \neq \beta$, the direction of the hopping is uniquely determined, and when $\alpha = \beta$ we take the hopping to the y direction. The phase factor $\phi'^{(m,n)}_{\mu\alpha\beta}$ ($m = n-1$ or $m = n+1$) is for the hopping μ from the β site in the nth unit cell to the α site in the mth unit cell ($4na \leqslant x_i < 4(n+1)a$ for the β site and $4ma \leqslant x_i < 4(m+1)a$ for the α site).

When the magnetic field is commensurate with the lattice period, i.e.,

$$\frac{\Phi}{\phi_0} = \frac{p}{q}, \tag{B17}$$

where p and q are integers, the magnetic unit cell is $4qa \times b$. The Hamiltonian is written as

$$\hat{\mathcal{H}} = \sum_{\mathbf{k}} \tilde{C}_{\mathbf{k}}^\dagger \tilde{\varepsilon}_{\mathbf{k}} \tilde{C}_{\mathbf{k}}, \tag{B18}$$

where the summation over $\mathbf{k}$ is taken in the magnetic Brillouin zone,

$$-\frac{\pi}{4qa} \leqslant k_x < \frac{\pi}{4qa}, \tag{B19}$$

$$-\frac{\pi}{b} \leqslant k_y < \frac{\pi}{b}, \tag{B20}$$

$\tilde{C}_{\mathbf{k}}^\dagger$ and $\tilde{C}_{\mathbf{k}}$ have $4q$ components of creation and annihilation operators:

$$\tilde{C}_{\mathbf{k}}^\dagger = \left(a_{\mathbf{k}}^{(0)\dagger}, b_{\mathbf{k}}^{(0)\dagger}, a_{\mathbf{k}}^{\prime(0)\dagger}, b_{\mathbf{k}}^{\prime(0)\dagger}, \cdots, a_{\mathbf{k}}^{\prime(q-1)\dagger}, b_{\mathbf{k}}^{\prime(q-1)\dagger}\right) \tag{B21}$$

and

$$\tilde{C}_{\mathbf{k}} = \begin{pmatrix} a_{\mathbf{k}}^{(0)} \\ b_{\mathbf{k}}^{(0)} \\ a_{\mathbf{k}}^{\prime(0)} \\ b_{\mathbf{k}}^{\prime(0)} \\ \vdots \\ a_{\mathbf{k}}^{\prime(q-1)} \\ b_{\mathbf{k}}^{\prime(q-1)} \end{pmatrix}. \tag{B22}$$

The $4q \times 4q$ matrix $\tilde{\varepsilon}_{\mathbf{k}}$ is expressed with 4×4 matrices $D_{\mathbf{k}}^{(n)}$ and $F_{\mathbf{k}}^{(n)}$ as

$$\tilde{\varepsilon}_{\mathbf{k}} = \begin{pmatrix} D_{\mathbf{k}}^{(0)} & F_{\mathbf{k}}^{(1)} & 0 & \cdots & 0 & F_{\mathbf{k}}^{(0)\dagger} \\ F_{\mathbf{k}}^{(1)\dagger} & D_{\mathbf{k}}^{(1)} & F_{\mathbf{k}}^{(2)} & \ddots & \ddots & 0 \\ 0 & F_{\mathbf{k}}^{(2)\dagger} & D_{\mathbf{k}}^{(2)} & F_{\mathbf{k}}^{(3)} & \ddots & \vdots \\ \vdots & \ddots & \ddots & \ddots & \ddots & 0 \\ 0 & \ddots & \ddots & F_{\mathbf{k}}^{(q-2)\dagger} & D_{\mathbf{k}}^{(q-2)} & F_{\mathbf{k}}^{(q-1)} \\ F_{\mathbf{k}}^{(0)} & 0 & \dots & 0 & F_{\mathbf{k}}^{(q-1)\dagger} & D_{\mathbf{k}}^{(q-1)} \end{pmatrix}, \tag{B23}$$

where

$$D_{\mathbf{k}}^{(n)} = \begin{pmatrix} \epsilon^{(n)}_{\mathbf{k}AA} & \epsilon^{(n)}_{\mathbf{k}AB} & \epsilon^{(n)}_{\mathbf{k}AA'} & 0 \\ \epsilon^{(n)}_{\mathbf{k}BA} & \epsilon^{(n)}_{\mathbf{k}BB} & \epsilon^{(n)}_{\mathbf{k}BA'} & \epsilon^{(n)}_{\mathbf{k}BB'} \\ \epsilon^{(n)}_{\mathbf{k}A'A} & \epsilon^{(n)}_{\mathbf{k}A'B} & \epsilon^{(n)}_{\mathbf{k}A'A'} & \epsilon^{(n)}_{\mathbf{k}A'B'} \\ 0 & \epsilon^{(n)}_{\mathbf{k}B'B} & \epsilon^{(n)}_{\mathbf{k}B'A'} & \epsilon^{(n)}_{\mathbf{k}B'B'} \end{pmatrix}, \tag{B24}$$

$$\epsilon^{(n)}_{\mathbf{k}AA} = 2t_{\mathrm{I}3}\cos\left[bk_y + 2\pi\phi^{(n)}_{\mathrm{I}3AA}\right] + V, \tag{B25}$$

$$\epsilon^{(n)}_{\mathbf{k}BB} = 2t_{\mathrm{I}3}\cos\left[bk_y + 2\pi\phi^{(n)}_{\mathrm{I}3BB}\right] + V, \tag{B26}$$

$$\epsilon^{(n)}_{\mathbf{k}A'A'} = 2t_{\mathrm{I}3}\cos\left[bk_y + 2\pi\phi^{(n)}_{\mathrm{I}3A'A'}\right] - V, \tag{B27}$$

$$\epsilon^{(n)}_{\mathbf{k}B'B'} = 2t_{\mathrm{I}3}\cos\left[bk_y + 2\pi\phi^{(n)}_{\mathrm{I}3B'B'}\right] - V, \tag{B28}$$

$$\begin{aligned}\epsilon^{(n)}_{\mathbf{k}AB} &= \epsilon^{(n)*}_{\mathbf{k}BA}\\ &= t_{\mathrm{S}1}e^{iak_x} + t_{\mathrm{I}1}\exp\left[i\left(ak_x - bk_y - 2\pi\phi^{(n)}_{\mathrm{I}1AB}\right)\right],\end{aligned} \tag{B29}$$

$$\begin{aligned}\epsilon^{(n)}_{\mathbf{k}BA'} &= \epsilon^{(n)*}_{\mathbf{k}A'B}\\ &= t_{\mathrm{S}2}e^{iak_x} + t_{\mathrm{I}2}\exp\left[i\left(ak_x - bk_y - 2\pi\phi^{(n)}_{\mathrm{I}2BA'}\right)\right],\end{aligned} \tag{B30}$$

$$\begin{aligned}\epsilon^{(n)}_{\mathbf{k}A'B'} &= \epsilon^{(n)*}_{\mathbf{k}B'A'}\\ &= t_{\mathrm{S}1}e^{iak_x} + t_{\mathrm{I}1}\exp\left[i\left(ak_x - bk_y - 2\pi\phi^{(n)}_{\mathrm{I}1A'B'}\right)\right],\end{aligned} \tag{B31}$$

$$\epsilon^{(n)}_{\mathbf{k}AA'} = \epsilon^{(n)*}_{\mathbf{k}A'A} = t_{\mathrm{I}4}\exp\left[i\left(2ak_x - bk_y - 2\pi\phi^{(n)}_{\mathrm{I}4AA'}\right)\right], \tag{B32}$$

$$\epsilon^{(n)}_{\mathbf{k}BB'} = \epsilon^{(n)*}_{\mathbf{k}B'B} = t_{\mathrm{I}4}\exp\left[i\left(2ak_x - bk_y - 2\pi\phi^{(n)}_{\mathrm{I}4BB'}\right)\right], \tag{B33}$$

$$F^{(n)}_{\mathbf{k}} = \begin{pmatrix} 0 & 0 & 0 & 0\\ 0 & 0 & 0 & 0\\ \epsilon'^{(n)}_{\mathbf{k}A'A} & 0 & 0 & 0\\ \epsilon'^{(n)}_{\mathbf{k}B'A} & \epsilon'^{(n)}_{\mathbf{k}B'B} & 0 & 0\end{pmatrix}, \tag{B34}$$

$$\epsilon'^{(n)}_{\mathbf{k}A'A} = t_{\mathrm{I}4}\exp\left[i\left(2ak_x - bk_y - 2\pi\phi'^{(n-1,n)}_{\mathrm{I}4A'A}\right)\right], \tag{B35}$$

$$\epsilon'^{(n)}_{\mathbf{k}B'B} = t_{\mathrm{I}4}\exp\left[i\left(2ak_x - bk_y - 2\pi\phi'^{(n-1,n)}_{\mathrm{I}4B'B}\right)\right], \tag{B36}$$

$$\begin{aligned}\epsilon'^{(n)}_{\mathbf{k}B'A} &= t_{\mathrm{S}2}\exp[iak_x]\\ &\quad + t_{\mathrm{I}2}\exp\left[i\left(ak_x - bk_y - 2\pi\phi'^{(n-1,n)}_{\mathrm{I}2B'A}\right)\right].\end{aligned} \tag{B37}$$

The matrix of Eq. (B23) can be numerically diagonalized.

[1] For a review, see T. Ishiguro, K. Yamaji, and G. Saito, *Organic Superconductors*, 2nd ed. (Springer-Verlag, Berlin, 1998).
[2] P. M. Grant, Phys. Rev. Lett. **50**, 1005 (1983).
[3] J. P. Pouget, R. Moret, R. Comes, and K. Bechgaard, J. Phys. (France) Lett. **42**, 543 (1981).
[4] D. Vignolles, A. Audouard, M. Nardone, and L. Brossard, S. Bouguessa, and J. M. Fabre, Phys. Rev. B **71**, 020404 (2005).
[5] W. Kang and Ok-Hee Chung, Phys. Rev. B **79**, 045115 (2009).
[6] D. Shoenberg, *Magnetic Oscillation in Metals* (Cambridge University Press, Cambridge, 1984).
[7] J. Y. Fortin and A. Audouard, Phys. Rev. B **77**, 134440 (2008).
[8] J. Y. Fortin and A. Audouard, Phys. Rev. B **80**, 214407 (2009).
[9] A. B. Pippard, Proc. Roy. Soc. A **270**, 1 (1962).
[10] L. M. Falicov and H. Stachoviak, Phys. Rev. **147**, 505 (1966).
[11] L. Onsager, Philos. Mag. **43**, 1006 (1952).
[12] M. Nakano, J. Phys. Soc. Jpn. **66**, 19 (1997).
[13] A. S. Alexandrov and A. M. Bratkovsky, Phys. Rev. B **63**, 033105 (2001).
[14] T. Champel, Phys. Rev. B **64**, 054407 (2001).
[15] K. Kishigi and Y. Hasegawa, Phys. Rev. B **65**, 205405 (2002).
[16] I. M. Lifshitz and A. M. Kosevich, Zh. Eksp. Teor. Fiz. **29**, 730 (1955) [Sov. Phys. JETP **2**, 636 (1956)].
[17] T. Champel and V. P. Mineev, Philos. Mag. B **81**, 55 (2001).
[18] I. A. Luk'yanchuk and Y. Kopelevich, Phys. Rev. Lett. **93**, 166402 (2004).
[19] I. A. Luk'yanchuk, Low Temp. Phys. **37**, 45 (2011).
[20] S. G. Sharapov, V. P. Gusynin, and H. Beck, Phys. Rev. B **69**, 075104 (2004).
[21] P. G. Harper, Proc. Phys. Soc. Lond. A **68**, 874 (1955).
[22] P. G. Harper, Proc. Phys. Soc. Lond. A **68**, 879 (1955).
[23] D. R. Hofstadter, Phys. Rev. B **14**, 2239 (1976).
[24] Y. Hasegawa, P. Lederer, T. M. Rice, and P. B. Wiegmann, Phys. Rev. Lett. **63**, 907 (1989).
[25] Y. Hasegawa, Y. Hatsugai, M. Kohmoto, and G. Montambaux, Phys. Rev. B **41**, 9174 (1990).
[26] K. Machida, K. Kishigi, and Y. Hori, Phys. Rev. B **51**, 8946 (1995).
[27] K. Kishigi, M. Nakano, K. Machida, and Y. Hori, J. Phys. Soc. Jpn. **64**, 3043 (1995).
[28] P. S. Sandhu, J. H. Kim, and J. S. Brooks, Phys Rev. B **56**, 11566 (1997).
[29] S. Y. Han, J. S. Brooks, and Ju H. Kim, Phys. Rev. Lett. **85**, 1500 (2000).
[30] V. M. Gvozdikov and M. Taut, Phys. Rev. B **75**, 155436 (2007).
[31] J. Y. Fortin and T. Ziman, Phys. Rev. Lett. **80**, 3117 (1998).
[32] K. Kishigi and K. Machida, Phys. Rev. B **53**, 5461 (1996).
[33] K. Kishigi and K. Machida, J. Phys.: Condens. Matter **9**, 2211 (1997).
[34] D. J. Thouless, M. Kohmoto, M. P. Nightingale, and M. den Nijs, Phys. Rev. Lett. **49**, 405 (1982).
[35] M. Kohmoto, Ann. Phys. (NY) **160**, 343 (1985).
[36] M. Kohmoto, Phys. Rev. B **39**, 11943 (1989).
[37] S. Tomic, J. R. Cooper, D. Jerome, and K. Bechgaard, Phys. Rev. Lett. **62**, 462 (1989).
[38] W. Kang, S. T. Hannahs, L. Y. Chiang, R. Upasani, and P. M. Chaikin, Phys. Rev. Lett. **65**, 2812 (1990).
[39] S. Tomic, J. R. Cooper, W. Kang, D. Jérome, and K. Maki, J. Phys. I France **1**, 1603 (1991).
[40] L. P. Le, A. Keren, G. M. Luke, B. J. Sternlieb, W. D. Wu, Y. J. Uemura, J. H. Brewer, T. M. Riseman, R. V. Upasani, L. Y. Chiang, W. Kang, P. M. Chaikin, T. Csiba, and G. Gruner, Phys. Rev. B **48**, 7284 (1993).
[41] K. Hiraki, T. Nemoto, T. Takahashi, H. Kang, Y. Jo, W. Kang, and O.-H. Cung, Synth. Met. **135-136**, 691 (2003).
[42] H. Satsukawa, K. Hiraki, T. Takahashi, H. Kang, Y. J. Jo, and W. Kang, J. Phys IV (France) **114**, 133 (2004).
[43] G. M. Danner, W. Kang, and P. M. Chaikin, Phys. Rev. Lett. **72**, 3714 (1994).
[44] T. Osada, S. Kagoshima, and N. Miura, Phys. Rev. Lett. **77**, 5261 (1996).

[45] H. Yoshino, K. Saito, H. Nishikawa, K. Kikuchi, K. Kobayashi, and I. Ikemoto, J. Phys. Soc. Jpn. **66**, 2410 (1997).
[46] I. J. Lee and M. J. Naughton, Phys. Rev. B **57**, 7423 (1998).
[47] A. G. Lebed and M. J. Naughton, Phys. Rev. Lett. **91**, 187003 (2003).
[48] K. Yamaji, J. Phys. Soc. Jpn. **58**, 1520 (1989).
[49] L. P. Gor'kov and A. G. Lebed', J. Phys. (Paris), Lett. **45**, 433 (1984).
[50] L. P. Gorkov and A. G. Lebed, Phys. Rev. B **51**, 3285 (1995).
[51] P. Alemany, J. P. Pouget, and E. Canadell, Phys. Rev. B **89**, 155124 (2014).
[52] Y. Barrans, J. Gaultier, S. Bracchetti, P. Guionneau, D. Chasseau, and J. M. Fabre, Synth. Met. **103**, 2042 (1999).
[53] Y. Hasegawa and M. Kohmoto, Phys. Rev. B **74**, 155415 (2006).
[54] K. S. Novoselov, A. K. Geim, S. V. Morozov, D. Jiang, M. I. Katsnelson, I. V. Grigorieva, S. V. Dubonos, and A. A. Firsov, Nature (London) **438**, 197 (2005).
[55] C. R. Dean, L. Wang, P. Maher, C. Forsythe, F. Ghahari, Y. Gao, J. Katoch, M. Ishigami, P. Moon, M. Koshino, T. Taniguchi, K. Watanabe, K. L. Shepard, J. Hone, and P. Kim, Nature (London) **497**, 598 (2013).
[56] Jesper Goor Pedersen and Thomas Garm Pedersen, Phys. Rev. B **87**, 235404 (2013).
[57] M. Aidelsburger, M. Atala, M. Lohse, J. T. Barreiro, B. Paredes, and I. Bloch, Phys. Rev. Lett. **111**, 185301 (2013).
[58] H. Miyake, G. A. Siviloglou, C. J. Kennedy, W. C. Burton, and W. Ketterle, Phys. Rev. Lett. **111**, 185302 (2013).
[59] A. Audouard, F. Goze, S. Dubois, J. P. Ulmet, L. Brossard, S. Askenazy, S. Tomić, and J. M. Fabre, Europhys. Lett. **25**, 363 (1994).
[60] M. Basletic, B. Korin-Hamzic, A. Hamzic, S. Tomic, and J. M. Fabre, Solid State Commun. **97**, 333 (1996).
[61] M. J. Naughton, J. P. Ulmet, I. J. Lee, and J. M. Fabre, Synth. Met. **85**, 1531 (1997).